# Pyrolysis of Tetraethoxysilane on Mo(100) at Low Temperatures

**T. A. Jurgens-Kowal and J. W. Rogers, Jr.***

*Department of Chemical Engineering, University of Washington, Seattle, Washington 98195-1750*

*Received: March 28, 1997; In Final Form: January 7, 1998*

Deposition of ultrathin silicon dioxide films on Mo(100) substrates by pyrolysis of tetraethoxysilane (TEOS) vapor has been investigated at temperatures between 300 and 860 K with X-ray photoelectron spectroscopy (XPS), temperature-programmed desorption (TPD), low-energy electron diffraction (LEED), and infrared reflection−absorption spectroscopy (IRRAS). Up to temperatures of ∼600 K, TEOS adsorbs on the Mo surface forming an ethoxysilyl intermediate, whereas at higher temperatures $SiO_2$ is formed during the initial exposure, as evidenced by both XPS and IRRAS data. Deposition of silicon dioxide is reaction-limited in the temperature range studied with roughly a monolayer forming on the surface at 860 K. Heating the TEOS-exposed Mo(100) surfaces to ∼1000 K yields ethylene as the predominant gas-phase decomposition product and improves both the stoichiometry and order of the films as indicated by an increase in the stretching frequency of the Si−O IRRAS peaks. A decrease in the amount of desorbed ethylene is observed as the deposition temperature increases from 300 to ∼600 K, and no significant desorption of any other decomposition products was detected at higher deposition temperatures. Carbon contamination is minimal in these $SiO_2$ films.

## I. Introduction

For many years, silicon dioxide has been used extensively in large-scale integrated circuits, such as bipolar and metal-oxide-semiconductor devices, because of its unique electrical and mechanical properties as an insulator. Tetraethoxysilane (TEOS) has gained popularity as a single-source precursor for $SiO_2$ since it has many desirable properties and oxides of high-quality can be produced by pyrolysis of TEOS at relatively low deposition temperatures.[1−9] Low deposition temperatures are often required in high-performance integrated circuits where multilevel interconnect technology demands both deposition of a metal layer (often Al as a conduction path) and of a dielectric.[10] Since the dielectric, or insulating layer, must be deposited on sharp metal lines without degradation of the metal or chemical reaction with the metal, the processing temperature is normally limited to <700 K to prevent diffusion between layers.[4,11] In addition, TEOS (1) incorporates oxygen in the single source precursor, (2) requires no special processing configurations in industrial chemical vapor deposition (CVD) systems such as injectors or caged boats,[1,2,9,12,13] and (3) is less hazardous than traditional vapor-phase sources such as silanes and chlorosilanes. Silicon dioxide films deposited by pyrolysis of TEOS show good uniformity and excellent step coverage. Under some conditions surfaces that initially show anisotropies can be smoothed using reflow techniques.[1,14] TEOS is one of a class of molecules called alkoxysilanes, which are of the form $(RO)_3SiOR'$ (where R, $R' = C_2H_5$ in TEOS). Films deposited by alkoxysilanes are also utilized in protective layer coatings, electronic sensors, chemically modified electrodes, thin film optics,[15] and antireflection coatings.[16−18] Interactions between Mo and $SiO_2$ are also of interest in order to better understand ceramic/metal interface properties, coating operations,[19,20] and reactions in heterogeneous catalysis, since $SiO_2$ is often used a catalyst support material.[20−28]

Although many empirical studies of TEOS pyrolysis have been reported,[1,6−8,10−13,29] the fundamental reactions of TEOS and $SiO_2$ film formation on well-defined transition-metal surfaces has not been previously addressed in detail. In addition, only a few studies have examined the growth of silicon dioxide on Mo single-crystal surfaces.[20,21,25,26] These investigations have indirectly demonstrated the usefulness of a single-source precursor in the deposition of silicon dioxide thin films. Xu et al. heated a block of Si in an oxygen atmosphere in order to deposit $SiO_2$ on Mo(100) and Mo(110). They found Si(2p) XPS features representative of Si (∼99 eV), suboxides (such as $Si_2O_3$), and $SiO_2$ (∼103 eV).[20,21,25] The former features were found to decrease substantially after a high-temperature anneal (∼1200−1400 K), leaving primarily $SiO_2$ on the surface.[20,21,25,26] These authors mention, however, that the choice of heating wire for the Si block is critical, as impurity atoms from the heating element were sometimes incorporated into the growing $SiO_2$ film.[21] Other studies reporting $SiO_2$ film formation by TEOS decomposition on Mo surfaces focused on reaction kinetics and thus examined only the properties of thick films (450 nm to 6 $\mu$m) and did not investigate substrate effects.[12,13]

In this paper we present fundamental studies of ultrathin silicon dioxide film formation by pyrolysis of TEOS vapor on a well-characterized, single-crystal transition-metal surface. Using X-ray photoelectron spectroscopy (XPS), temperature-programmed desorption (TPD), low-energy electron diffraction (LEED), and Fourier-transform infrared reflection−absorption spectroscopy (IRRAS) as diagnostics, we examined the adsorption and thermal decomposition of TEOS to form thin silicon dioxide films on Mo(100) for deposition temperatures ranging from 300 to 860 K. We then characterized the composition, thickness, and structure (both local and long-range) of these films as a function of deposition temperature.

## II. Experiment

Experiments were performed in a dual-level stainless steel ultrahigh vacuum (UHV) chamber. Details of this reaction chamber, which models a traditional cold-wall chemical vapor deposition (CVD) reactor, have been presented previously.[30] The chamber is continuously pumped to the mid-$10^{-10}$ Torr range

S1089-5647(97)01098-5 CCC: $15.00 
Published on Web 02/25/1998

by two turbomolecular pumps (Balzers; TPU 330 and TPU 060), with additional pumping provided by an ion pump (Perkin-Elmer; Ultek 350MA). In brief, the upper level is equipped with an X-ray gun (Leybold; RQ-20−63) and hemispherical analyzer (VSW; Class 150) for XPS, a quadrupole mass spectrometer (UTI; Model 100C) and temperature controller (Eurotherm; 906S) interfaced to a computer for TPD, and LEED optics (Varian; model 981-0127). In addition, an $Ar^+$ ion sputter gun (LK Technologies; NGI-3000-SE) is available on the upper level for cleaning the single-crystal molybdenum surface. The lower level functions as a high-pressure cell and is equipped with differentially pumped KBr windows to facilitate infrared analysis (Mattson; Galaxy 5020). The polished Mo(100) sample (1 cm in diameter and ∼0.5-mm thick) was mounted with 0.5 mm diameter tantalum wires to a gold-plated substrate holder, attached to an UHV feedthrough containing two copper electrical leads and a W-5% Re/W-26% Re thermocouple. The thermocouple is spot-welded to the back of the sample, and the temperature was readily monitored as the sample could be heated resistively to ∼1000 K. A 0.5-mm diameter tantalum wire, mounted on a translational motion bellows, served as an electron beam filament to accommodate heating the sample to ∼2000 K. Tetraethoxysilane (Aldrich, 99+%) is a liquid at room temperature and was contained in a glass vial attached to a stainless steel gas-handling manifold, which incorporates a leak valve on each level of the chamber. The vapor pressure of TEOS at room temperature is ∼1.2 Torr, and its purity was verified periodically by mass spectrometry.[31−34] TEOS was dosed only after several liquid nitrogen freeze−pump−thaw cycles and after flushing the gas-handling system several times with TEOS vapor in order to passivate the tube walls against undesired reactions and to prevent contamination.

A clean Mo(100) surface was obtained by $Ar^+$ ion sputtering (1.5 kV, ∼6 $\mu$A), followed by electron beam heating to ∼2000 K. After this cleaning procedure, the sample produced a sharp, bright (1 × 1) LEED pattern and showed no carbon contamination by XPS. However, some surface oxygen was not removed by this procedure and was always present in the XPS spectra at a binding energy of ∼530 eV. This was easily distinguished from features induced by TEOS and its reaction (see below). This minority oxygen species may result from diffusion from the bulk to the Mo(100) surface, although the molybdenum surface itself was not oxidized because no XPS peak shifts were detected for the $Mo(3d)_{5/2}$ feature at 228.0 eV. (Peak shifts of 1.6 and 4.8 eV are expected for $MoO_2$ and $MoO_3$, respectively,[35,36] and oxidation of molybdenum is known to occur only at high temperature.[21]) This surface oxygen remains unreactive to TEOS and has no direct effect on the pyrolysis reactions or formation of $SiO_2$ on the Mo surface. There was no correlation between the final Si(2p) intensity in the $SiO_2$ films and the initial O(1s) peak at ∼530 eV. TEOS was exposed to the Mo(100) surface at predetermined temperatures in the high-pressure cell in order to reduce contamination of the chamber's upper level. Exposures were carried out for 15 min at a corrected ion gauge pressure of $\sim 4 \times 10^{-7}$ Torr.[37] Typically, the reaction pressure and temperature stabilized within 3−4 min, and the chamber could be evacuated to $< 1 \times 10^{-8}$ Torr in ∼2 min following TEOS exposures. For XPS and TPD measurements, the sample was removed to the upper level, while for IRRAS analysis, the sample was held at the lower level throughout the analysis, since this technique is very sensitive to sample position.

XPS and LEED characterizations were performed on the clean surface, after TEOS deposition and after TPD. The spectrometer was operated with a Mg(Kα) X-ray source and FAT = 44, such that the fwhm of the $Mo(3d)_{5/2}$ peak was 1.4 eV, which can be considered the working resolution of this instrument. Unless otherwise indicated, XPS spectra were obtained at a takeoff angle of 60°, defined as the angle between the surface normal and the entrance to the hemispherical analyzer. Binding energies were calibrated to the Fermi energy of gold {$Au(4f)_{7/2}$ peak at 83.8 eV},[35] and peak intensities were normalized to the $Mo(3d)_{5/2}$ peak area. TPD experiments were performed by ramping the sample at a linear rate of 3 K/s from room temperature to a maximum of 1020 K. The sample was typically held at this upper temperature for a 15-s anneal. Up to 10 masses were recorded in a typical TPD experiment, which included some combination of $m/e$ = 2, 12, 14, 16, 18, 26, 27, 28, 29, 31, 32, 44, 60, 63, and 79. These masses represent ions of the parent molecule and of expected decomposition products. Quantitative TPD analysis included corrections to the spectra for experimentally determined cracking patterns, ionization efficiency, and the transmission and electron multiplier gain of the mass spectrometer. Cracking patterns were experimentally measured for the following desorption products: acetaldehyde, $CO_2$, diethyl ether, ethanol, and ethylene; the quadrupole manufacturer's cracking pattern data were used for acetylene, ethane, methane, butene, and methanol. IRRAS experiments were performed at an 85° angle of incidence, using a 100-kHz travel frequency for the moving mirror, 8 $cm^{-1}$ resolution and 4000 scans, and the beam path was purged with dry nitrogen. IRRAS data were recorded as single-beam spectra; a single spectrum could be collected in approximately 7 min, such that background and purge effects were minimized. No polarization of the incident beam was utilized as the metal surface selection rule was in effect for our experimental configuration.[38−46] IRRAS data are illustrated in this paper as transmittance ($T$) as a function of wavenumber, according to the relation[45,47]

$$T = \left[\frac{(R_{ads} - R_{clean})}{R_{clean}}\right] \quad (1)$$

where $R_{clean}$ represents the single-beam spectrum of the clean Mo(100) surface and $R_{ads}$ is the single-beam spectra after TEOS/$SiO_2$ deposition.

## III. Results

**A. XPS.** Figure 1 shows high-resolution XPS spectra of the Si(2p), O(1s), and C(1s) binding-energy regions for TEOS depositions at 380 and 780 K (curves a and b, respectively). The data illustrated is raw data, except for a Shirley background subtraction;[48] thus, comparison of peak intensities as shown must be done with care. The peak maximum of the Si(2p) signal is ∼103 eV, which is the reported binding energy for {$SiO_4$} species, where silicon atoms are tetrahedrally bonded to four oxygen atoms.[20,22,35] As can be readily seen from Figure 1A, the Si(2p) intensity is significantly greater for the higher deposition temperature, as is the O(1s) signal intensity, shown in Figure 1B. In addition, the Si(2p) peak position is nearly 1 eV higher in binding energy for the 780 K deposition vs that at lower temperature. A binding energy of ∼103 eV is consistent with literature values for the Si(2p) peak position in $SiO_2$.[20,21,28,35,49,50] Surface oxygen, which was always present on the Mo(100) crystal (see above), can be observed as the low-binding-energy shoulder in Figure 1B. The fwhm of the O(1s) signal is greater than 4 eV, indicating the presence of two types of oxygen, such that peaks at ∼532 and ∼530 eV can be readily resolved. As will be discussed below, the peak at ∼532 eV was found to increase with deposition temperature and is linearly

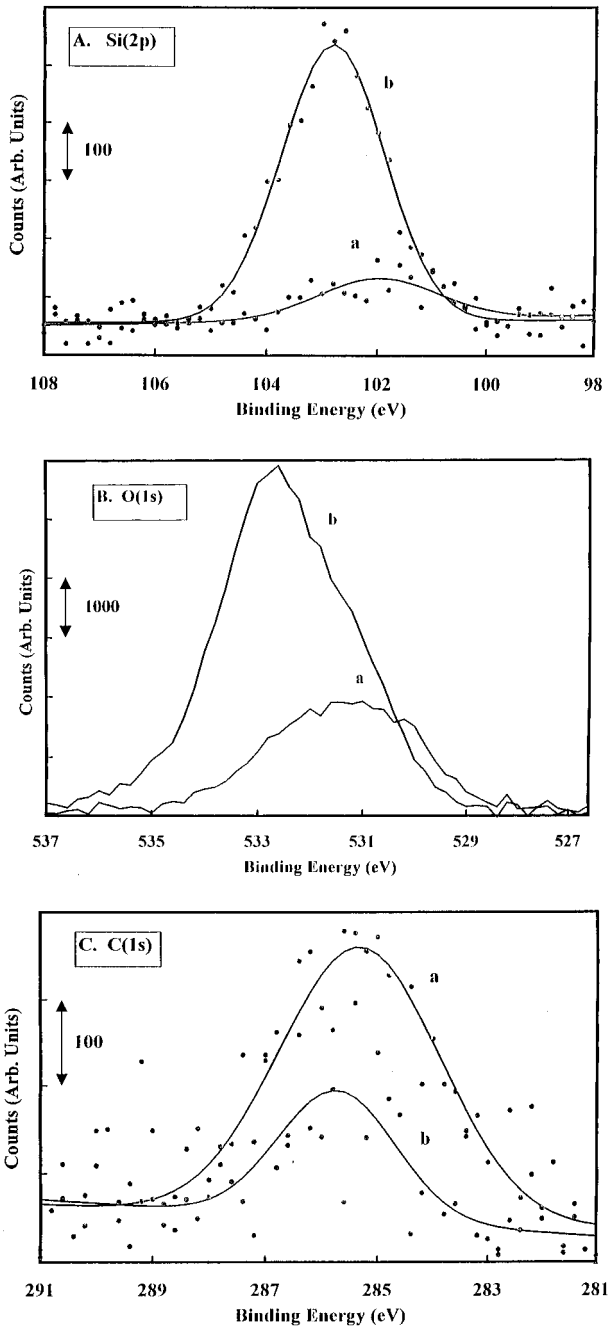


**Figure 1.** High-resolution XPS spectra for the (A) Si(2p), (B) O(1s), and (C) C(1s) binding-energy regions for TEOS as-deposited on Mo-(100). Curves a and b are representative of low- and high-temperature depositions at 380 and 780 K, respectively.

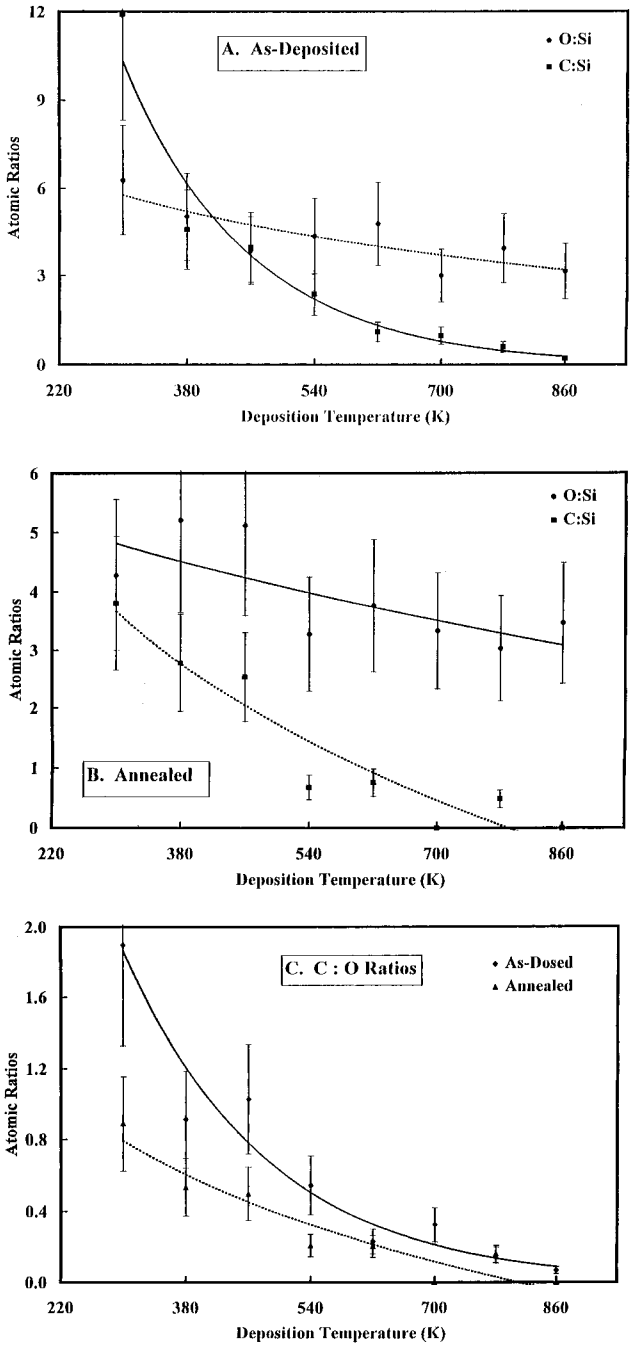


**Figure 2.** Atomic ratios of O:Si (◆) and C:Si (■) for the as-deposited TEOS film (A) and after heating the surface to ∼1000 K (B), and (C) the C:O atomic ratios for as-dosed (◆) and annealed (▲) TEOS films. (The error bars are ±30%.)

correlated to the intensity increases of the Si(2p) peak, whereas the peak at ∼530 eV shows no change in relative intensity as a function of TEOS deposition and is not correlated to either the Si(2p) or C(1s) peaks on the as-dosed or annealed Mo(100) surfaces. Furthermore, an O(1s) binding energy of ∼532 eV is indicative of an oxide species in which the oxygen is tetrahedrally coordinated to Si.[20,28,35] The C(1s) fwhm is also greater than 4 eV (Figure 1C), and two peaks can be resolved at ∼284.5 and 286.5 eV. These peaks have previously been assigned to the methyl and alcoholic carbon atoms, respectively, in the ethoxy ligand.[35,49,51,52] Note that at the lower deposition temperature, more carbon is present on the surface, indicated by a greater C(1s) peak intensity as shown in Figure 1C, curve a, whereas the surface carbon is greatly reduced for a TEOS deposition at 780 K. We observed no change in the fwhm or binding energies of the Mo(3d) peaks after TEOS/$SiO_2$ deposition, which is in agreement with previous studies of silica thin film formation on Mo(100), thus indicating that the molybdenum surface is not oxidized by reaction with the TEOS.[20]

These trends are illustrated in Figure 2, where we show the O(1s) and C(1s) peak intensities normalized to the Si(2p) intensity as a function of the TEOS deposition temperature. Atomic ratios ($n_1/n_2$) are calculated according to eq 2, where $I$ is the peak intensity, which is corrected for the XPS sensitivities, $S_i$:[35,53−55]

$$\frac{n_1}{n_2} = \frac{(I_1/S_1)}{(I_2/S_2)} \qquad (2)$$

The sensitivity can be defined as a function of the photoemission cross section, $d\sigma/d\Omega$; the inelastic mean free path (IMFP), $\lambda$; and the transmission efficiency of the spectrometer, *T(E)*; where the sample area irradiated and the X-ray flux are taken as constants:[53−55]

$$S = (d\sigma/d\Omega)\cdot\lambda\cdot T(E) \quad (3)$$

The transmission efficiency of the spectrometer is proportional to the inverse square root of energy,[54] the IMFP is calculated for inorganic compounds according to Seah and Dench,[56] and $d\sigma/d\Omega$ is calculated according to Yeh and Lindau.[57] On the basis of the approximate nature of the IMFP and *T(E)*, we estimate the atomic ratios calculated using these sensitivities to be within ±30%. (A 30% error is reasonable on the basis of the aggregate error involved in estimating *S*. First, the spread of values reported for the IMFP is 1.70,[56] and errors of 20% or greater are not uncommon when the IMFP is used to calculate the distance an emitted photoelectron travels through an overlayer.[54] Second, the photoionization cross section is accurate to within 10%,[57] and finally, the greatest contribution to sensitivity factor may be the estimation of the transmission efficiency. Transmission efficiency is best determined by measuring a variety of spectral features on each spectrometer, although many empirical relations abound in the literature.[54] $T(E)$ is often reported to be inversely related to the square root of the kinetic energy of a photoemitted electron; however, the relation is occasionally reported as $T(E)$ proportional to the inverse of the kinetic energy.[54] This results in a 30% error in the sensitivity alone, if one calculates $T(E)$ by the two different methods for a 1000-eV electron.)

As shown in Figure 2A, TEOS deposition at 300 K leads to C:Si and O:Si atomic ratios expected for the molecular species. (Note that because the silicon signal was quite small and is detected at relatively low binding energy and because Si atoms may be shadowed by ethoxy groups, the error bars are greatest for the lowest temperature depositions. We have observed a similar shadowing effect for TEOS deposited on $TiO_2$(110).[49]) At the lower deposition temperatures, the C:Si atomic ratio is approximately 8 (within the error bars), which agrees well with the C:Si atomic ratio in molecular TEOS. Similarly, the O:Si ratio for TEOS deposition on the clean Mo(100) surface is approximately 4. As the deposition temperature increases, the relative signal intensities of the C(1s) and O(1s) features decrease (Figure 1), and at the highest deposition temperatures, little carbon is deposited with the film. The O:Si atomic ratio approaches an expected value of 2 for silicon dioxide formation at these higher deposition temperatures.

In Figure 2B, we show atomic ratios, O:Si and C:Si, as a function of deposition temperature after heating the TEOS-exposed molybdenum surfaces to ∼1000 K. A similar trend to that of Figure 2A is shown, where the C:Si and O:Si ratios decrease with increasing deposition temperature. In addition, the C:Si ratio is about 40−60% less on the annealed samples than the as-dosed values for low-temperature depositions. On the other hand, the C:Si atomic ratio changes little in the high-temperature region, where only a minimal amount of carbon is initially deposited (Figure 1C, curve b). Similarly, the O:Si ratio changes little in the high-temperature regime as a result of annealing the TEOS-exposed Mo samples and maintains a value of approximately 2. In the lower temperature region, the O:Si ratio remains approximately 4, showing that the carbon is retained via an oxygen bond and probably in the form of a diethoxysilyl surface intermediate. These intermediates have previously been observed for TEOS deposition on $TiO_2$,[48,58] $SiO_2$,[2,59,60] and Si(100) surfaces.[61] We will discuss the nature of the surface intermediate in the next section.

Shown in Figure 2C are the C:O atomic ratios calculated from the data presented in Figure 2A,B. After a TEOS exposure at 300 K, we observe a C:O atomic ratio of about 2, but increasing the deposition temperature to above room temperature yields a C:O atomic ratio of about 1, and at deposition temperatures above ∼600 K, the C:O ratio is less than ∼20%. This indicates that although oxygen is being deposited on the surface, little carbon is incorporated in the film, as indicated by Figures 1C and 2A. After the surfaces are heated to ∼1000 K for TPD, the C:O ratio drops about 40−60% from the as-dosed atomic ratios. At a deposition temperature of 300 K, followed by heat treatment, the remaining surface C:O atomic ratio is approximately 1, indicating that if all of the oxygen originally deposited in the TEOS exposure remained on the surface, half of the carbon would be removed during the heat treatment. This implies a diethoxysilyl surface species and is in agreement with the Si(2p) binding energy and with our TPD and IRRAS data (see below). As for the C:Si atomic ratios, the C:O atomic ratio in Figure 2C does not show any significant variation for deposition temperatures above ∼600 K, since only minimal carbon is detected on the Mo(100) surface for these films anyway (see Figures1C and 3C).

Figure 3A−C shows the corresponding high-resolution Si(2p), O(1s), and C(1s) XPS scans, for TEOS depositions on Mo(100) at 380 and 780 K (curves a and b, respectively) after heating to ∼1000 K. TPD was performed in conjunction with this heat treatment and is discussed in the next section. Corresponding to the as-dosed case, the Si(2p) and O(1s) signal intensities are also greater at the higher temperature deposition, whereas the lower temperature deposition shows a greater amount of residual carbon after heat treatment. Similarly, it should be noted that the Si(2p) binding energy after annealing is ∼103 eV for the film initially exposed at 780 K, whereas the binding energy is closer to ∼102 eV for the film deposited at a lower temperature. Thus, at a higher deposition temperature, the Si(2p) binding energy is indicative of $SiO_2$ formation, whereas at the lower deposition temperature, the Si(2p) binding energy can be identified with an ethoxysilane species with bonding in the form of Si−O−C.[35,62] (See Section IIIC, below.) In any case, the Si is present in a +4 oxidation state because no XPS intensity was detected at a binding energy lower than ∼102 eV, where Si(2p) peaks for the metal (∼99 eV) or for silicon in a single oxidation state would be expected.[20] The apparent increases of the Si(2p) and O(1s) signals for the 380 K deposition (Figure 3A, curve a) after heat treatment have two possible explanations. The first is due to occasional and random signal fluctuations as a result of slight sample misalignment or instrument variations. The second explanation is that ethoxy groups of the diethoxysilyl intermediate may be shadowing the Si and O atoms at the given takeoff angle. It is for these reasons that we have only made relative comparisons for Si(2p) and O(1s) normalized to the $Mo(3d)_{5/2}$ peak area. Note that in Figure 3A, as the deposition temperature increases, the Si(2p) peak binding energy increases by ∼1 eV, indicating that at higher deposition temperatures, the silicon is more likely bound to oxygen in an oxide environment compared to the tetrahedral bonding found in the ethoxysilane species, as observed for the lower deposition temperatures.

It is also apparent, from Figure 3B, that there is a greater amount of oxygen deposited on the molybdenum surface at the higher deposition temperatures (see Figure 2 also). In addition, curve a shows that the O(1s) signal for TEOS deposition at

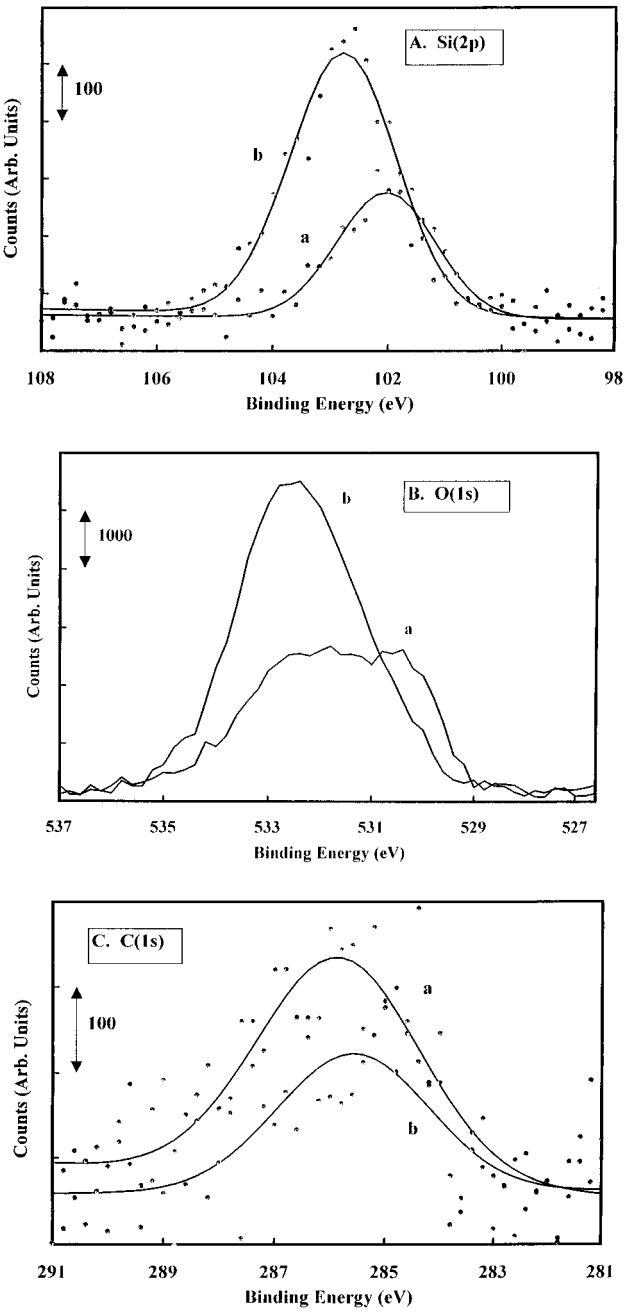


**Figure 3.** High-resolution XPS spectra for the (A) Si(2p), (B) O(1s), and (C) C(1s) binding-energy regions for TEOS films after heat treating to ~1000 K. Curves a and b are representative of low- and high-temperature depositions at 380 and 780 K, respectively.

380 and 780 K after annealing has a fwhm greater than 4 eV. Again, two peaks are easily resolved at ~530 and ~532 eV. The latter peak position is consistent with the formation of an oxide film.[20,35] The relative amount of oxygen deposited for the lower temperature deposition case is less than that for the higher deposition temperatures (Figure 3B). This, as well as the more intense Si(2p) signal (Figure 3A, curve b), is indicative of more $SiO_2$ growth at higher deposition temperatures. We will discuss the thickness and continuity of the $SiO_2$ films in greater detail in the next section.

**B. TPD.** Parts A and B of Figure 4 show the $m/e = 26$ and $m/e = 31$ TPD spectra for TEOS depositions at 380 K (curves a) and 780 K (curves b), respectively. These spectra represent desorption of ethylene and ethanol from the TEOS-exposed Mo(100) surfaces and are displaced along the *y*-axis for clarity. (We have chosen to follow $m/e = 26$ as a representative ion for $C_2H_4$ rather than $m/e = 28$, which may have contributions from CO, and $m/e = 31$ as a representative ion for $C_2H_5OH$ since TEOS has a strong mass fragment at $m/e = 45$ and $m/e = 46$ is somewhat weaker in intensity than $m/e = 26$.) Ethylene is the primary desorption product observed in TPD. This agrees well with other studies of TEOS decomposition on semiconductor and metal oxide surfaces.[2,3,8,13,16,29,49,58−61,63,64] We have carefully examined the TPD spectra for other predicted decomposition products including water ($m/e = 18$), diethyl ether ($m/e = 59$), ethane ($m/e = 30$), and SiO ($m/e = 44$) though we observed no significant desorption for any of these species. (Silicon monoxide has previously been observed in TPD spectra from Mo(100) and (110) surfaces where $SiO_2$ thin films were deposited by evaporation of Si in an oxygen atmosphere.[20,21,25,26]) The $m/e = 18$ signal, however, steadily increased (5−10%) over the temperature range probed (300−1000 K), but with no specific desorption features. Water could potentially be a reaction product,[8,13,65] but the increase in the $m/e = 18$ signal is more likely a function of convective heating of the gases in the vicinity of the hot sample and the mass spectrometer. A small amount of molecular TEOS desorption was observed at ~315 K.

Ethylene desorption, shown in Figure 4A by $m/e = 26$, was also indicated by the $m/e = 14$ and $m/e = 28$ TPD spectra (not shown). We observed $m/e = 14$ and $m/e = 28$ TPD features corresponding in peak shape and temperature to the $m/e = 26$ desorption features, providing further evidence that the $m/e = 26$ TPD spectrum is due to ethylene desorption. The presence of $m/e = 14$ is likely due to $CH_2$, a fragmentation product of ethylene that can be formed within the mass spectrometer, and $m/e = 28$ is the parent ion.[34] For purposes of quantitating the desorption yield, we have fit the peak intensity for the $m/e = 26$ TPD spectra with three curves, centered at ~550, 675, and 850 K (identified as peaks $\alpha$, $\beta$, and $\gamma$), and the $m/e = 31$ spectra with a single curve. The $\alpha$ and $\beta$ curve fits are not unique but are consistent with previously observed broad ethylene and ethanol desorption features from dehydroxylated and water-predosed $TiO_2$ surfaces subsequently exposed to TEOS[49,58] and with ethylene desorption from diethoxysilyl intermediates formed by TEOS decomposition on amorphous, hydroxylated $SiO_2$ surfaces.[2,4,59,64] Ethylene desorption was also observed from TEOS-exposed Si(100)-(2 × 1) surfaces at ~500, 600, and 720 K.[4,63] The lower temperature desorption feature was attributed to ethyl groups on the ethoxysilane intermediate undergoing $\beta$-hydride elimination, and the second peak attributed to desorption of di-$\sigma$-ethylene from the Si(100) surface. The highest temperature desorption feature was assumed to be ethylene stabilized on the Si surface by nearby adsorbed hydrogen atoms.[63] The difference in the peak temperature of the latter desorption feature on Mo(100) and Si(100) may be due to different stabilization mechanisms on these two surfaces.

There are several important points to note in Figure 4. Ethylene is known to adsorb molecularly on Mo(100) surfaces at 80 K, but heating leads to carbon−carbon bond scission, with no molecular $C_2H_4$ remaining on the surface above room temperature.[63,66,67] Thus, the ethylene that is observed in the TPD spectra of Figure 4A must be due to decomposition reaction of either molecular TEOS or of ethoxysilyl intermediates, as previously observed.[2,16,49,58−60,64] Similarly, alcohols adsorbed on molybdenum and molybdenum oxide surfaces below room temperature are known to decompose to alkoxide intermediates by ~300 K, with no molecular species remaining on the surface at or above room temperature.[67−69] By extension, then, the

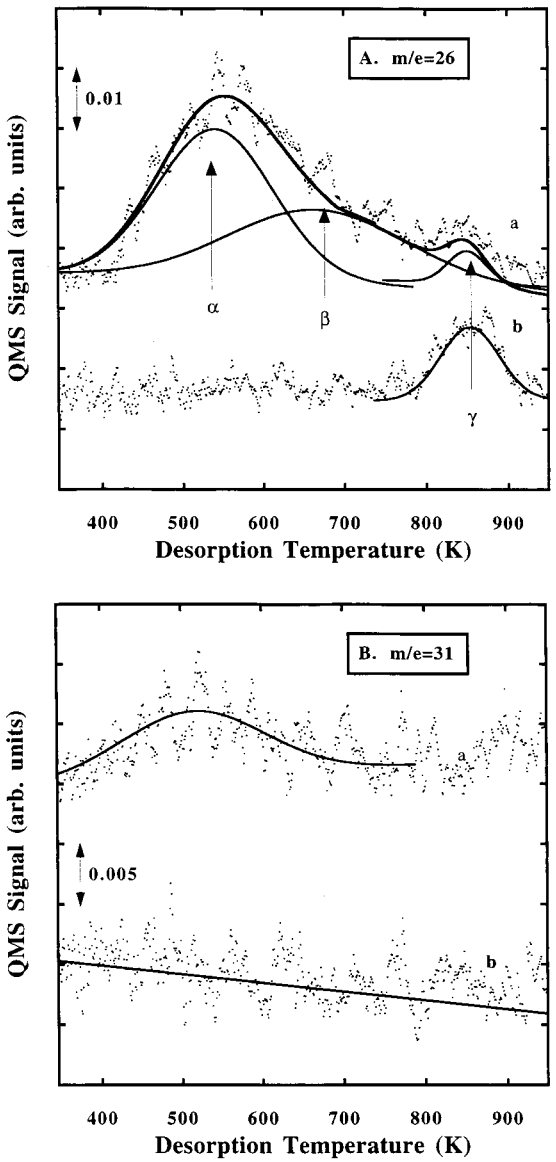


**Figure 4.** TPD spectra of (A) ethylene and (B) ethanol. Curves a and b represent TEOS depositions at 380 and 780 K, respectively.

ethanol observed in the TPD spectra of Figure 4B must also be formed via decomposition of TEOS and/or the ethoxysilyl intermediates. The second significant item observed in Figure 4 is that total desorption product yield is greater for surfaces exposed to TEOS at lower temperatures vs those at higher temperatures. This is not surprising since higher deposition temperatures lead to decomposition and desorption of byproduct species during the dosing process. Ethanol desorption is observed for surfaces dosed at less than ~600 K (Figure 4B, curve a), but at the higher deposition temperature, no ethanol is formed as a TPD desorption product (curve b).

These trends are further illustrated in Figure 5 and Table 1, where we show the total $C_2$ and the relative desorption product yield as a function of TEOS deposition. The desorption product yield was calculated by the sum of the α, $\beta$, and $\gamma$ peak areas fit to the $m/e = 26$ spectra and to the single-peak fit to the $m/e = 31$ feature. The total absolute peak intensity of the $m/e = 26$ and $m/e = 31$ desorption features from the TPD spectra for the TEOS deposition at 300 K was normalized to 4, representing the total number of $C_2$ decomposition products possible for a single TEOS molecule, as shown in Figure 5. This assumes only that no TEOS decomposition and desorption of byproducts

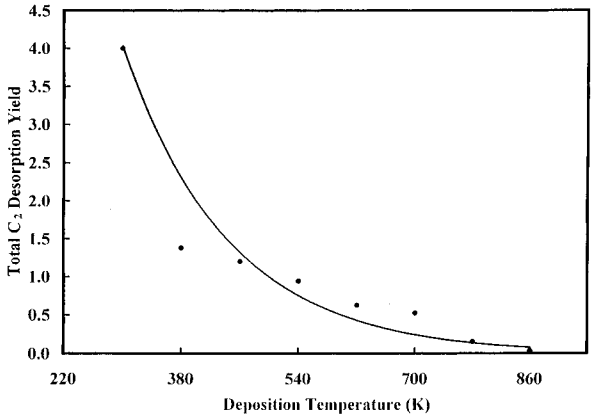


**Figure 5.** Total $C_2$ desorption product yield as a function of TEOS deposition temperature (see text).

**TABLE 1: Relative Desorption Product Yield**

| TEOS deposition temp (K) | ethylene | | | ethanol |
|---|---|---|---|---|
| | peak α | peak $\beta$ | peak $\gamma$ | |
| 300 | 1.46 | 1.43 | 0.70 | 0.41 |
| 380 | 0.69 | 0.47 | 0.05 | 0.16 |
| 460 | 0.47 | 0.58 | 0.04 | 0.11 |
| 540 | 0.10 | 0.54 | 0.16 | 0.15 |
| 620 | | 0.50 | 0.13 | |
| 700 | | 0.31 | 0.21 | |
| 780 | | | 0.16 | |
| 860 | | | 0.04 | |

accompanies adsorption at 300 K, which is further discussed in Section IV.A.3. The smooth curve shown in Figure 5 is provided simply to guide the eye.

Table 1 shows that ethylene desorption at ~550 K, peak α, represents the most significant contribution to the TPD spectra for TEOS depositions at low temperatures. The intensity of peak α decreases with increasing deposition temperature and completely disappears for TEOS exposures above ~600 K. Ethylene and ethanol, both desorbing at ~675 K (peak $\beta$), decrease in intensity with increasing deposition temperature. Desorption features for ethylene (peak $\beta$) and ethanol are not observed for Mo surfaces exposed to TEOS at higher temperatures. Previously, we (and others) have observed simultaneous ethylene and ethanol TPD features at ~650 K, attributed to $\beta$-hydride elimination on ethoxy-derivatized $TiO_2$ surfaces,[49,51,58,70] according to

$$2OEt_s \rightarrow C_2H_{4,g} + EtOH_g + O_s \qquad (4)$$

The subscript s refers to surface species, the nature of which we will discuss in the following section. Additional ethylene may be produced in this temperature range by desorption of di-$\sigma$-ethylene species, as has been observed on Si(100) surfaces.[63]

The only other TPD features that are significant (for higher temperature depositions only) are a $m/e = 26$ peak at ~850 K (peak *C*) and a $m/e = 28$ feature that initiates at ~1000 K (discussed below). The feature at ~850 K is present for all TEOS deposition temperatures studied here, and its relative desorption yield is approximately constant at about 0.2 (relative to the total $C_2$ desorption products for a room-temperature TEOS deposition). According to Figure 5, there are approximately 0.5 $C_2$ groups desorbing from surfaces exposed to TEOS at high deposition temperatures (>600 K, see Figure 2A, where our XPS results show a C:Si ratio of about 1). This is in agreement with one or less surface ethoxide groups, as in a monoethoxysilyl

surface intermediate. As shown in Figure 2B, the heat treatment reduces the C:Si ratio in proportion to the removal of ~0.5 $C_2$ groups (see Figure 5). On the basis of these data, we can envision a TEOS exposure at higher deposition temperatures primarily depositing $SiO_2$, with a few random ethoxy groups still bound to the central silicon atom, as in a monoethoxysilyl surface intermediate. The heat treatment to ~1000 K then removes these residual ethoxy groups as ethylene, which desorbs at ~850 K. Ethylene has previously been observed near this temperature for TEOS-exposed Si(100)-(2 × 1) surfaces.[63] Our IRRAS data (see below) offers further credence to this argument.

We also observe the onset of $m/e = 28$ desorption at ~1000 K (not shown here). (Unfortunately, our TPD spectra were not continued beyond a temperature of ~1020 K in order to limit high-temperature degradation of the sample support.) TPD features for $m/e = 28$ at ~1000 K have been attributed to CO desorption by recombination of C and O atoms on molybdenum surfaces.[21,67,71−75] We have observed similar features in the $m/e = 28$ TPD spectrum for Mo(100) surfaces exposed to carbon monoxide at ~100 and ~300 K. As expected, we also observe identical features in the $m/e = 12$ TPD spectra, which we attribute to atomic carbon, as well. It is likely that these species are a result of ionization of the gas-phase carbon monoxide to atomic carbon and oxygen in the mass spectrometer itself. Hence, we assign the $m/e = 28$ feature at ~1000 K to CO desorption due to recombination of atomic carbon and oxygen on the surface.

**C. IRRAS.** Infrared spectroscopy (IR) is a powerful tool for understanding solid-state interactions at coverages as low as submonolayer and without adverse effects due to charged particle probes.[41,50] In addition, the contour of the vibrational spectra is sensitive to chemical bonding and the nature of adsorbates. As such, differences in IR spectra of low-temperature $SiO_2$ films have been utilized extensively for characterizing glass and insulating films on silicon.[47,50,65,76] Additionally, IR is an attractive in situ method in which materials, such as heterogeneous catalysts, can be studied as a function of temperature and sample properties, such as thickness and state of hydration or oxidation.[24,50]

Vibrational bands in the low-wavenumber (1300−900 $cm^{-1}$) region are assigned primarily to stretching vibrations of bonds containing carbon, oxygen, and silicon atoms or groups of these atoms: $\nu$(C−O), $\nu$(Si−O), and $\nu$(Si−O−C). In the IR region between ~1111 and 1000 $cm^{-1}$, alkoxysilanes typically have very strong vibrational bands.[31,77,78] For disiloxanes, this band may be found in the region ~1124−1020 $cm^{-1}$, while for tri- or tetrasiloxanes, this band may split into two or more overlapping components.[31] In particular, the infrared spectra of ethoxysilanes (such as triethylethoxysilane, triethoxyethylsilane, and TEOS) show a cluster of bands in the 1055−1120 $cm^{-1}$ region.[79] In Figure 6, we show the gas-phase transmission FTIR spectrum of TEOS. By comparison with published spectra of liquid-phase TEOS,[31,80−82] we have previously assigned the vibrational bands for gas-phase TEOS.[58] The band at 1175 $cm^{-1}$ and the feature at 1090 $cm^{-1}$ are attributed to the doublet stretching vibration of the Si−O−C functionality,[15] while the peak at ~1113 $cm^{-1}$ may be attributed to the stretching frequency of the C−O bond.[4,83] These assignments are in good agreement with those made for $SiO_2$ films deposited by a TEOS plasma, where features at 1170, 1120, and 1085 $cm^{-1}$ in the Si−O stretching region were attributed to interactions of residual $C_2H_5$ groups.[50] Although the features at 1060 and ~970 $cm^{-1}$ are not obvious from the raw data displayed in Figure 6, these features are distinct for the deconvoluted spectra fit by Gaussian

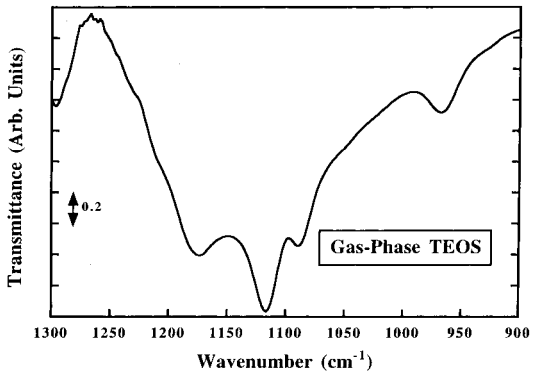


**Figure 6.** Gas-phase FTIR transmission spectrum of TEOS, at a pressure of 1 Torr, 4 $cm^{-1}$ resolution, 64 scans.

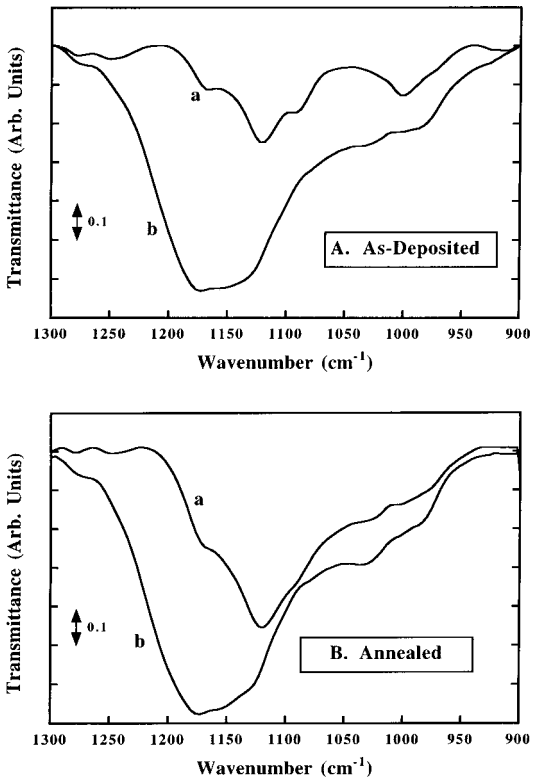


**Figure 7.** IRRAS spectra of TEOS films on Mo(100): (A) as-deposited and (B) after annealing to ~1000 K. Curves a and b are representative of low- and high-temperature depositions at 380 and 780 K, respectively.

curves. These vibrations can be attributed to stretching interactions of the Si−O bond.[15,81,82,84,85] The feature at ~1300 $cm^{-1}$ is assigned to a $CH_2$ bending mode.[58]

In Figure 7A are shown the IRRAS vibrational features in the Si−O stretching region (1300−900 $cm^{-1}$) for 380 K (curve a) and 780 K (curve b) TEOS depositions on Mo(100); data for the annealed surfaces are shown in Figure 7B. Note that the spectrum shown in Figure 7A, curve a, strongly resembles the gas-phase transmission IR spectrum for TEOS (Figure 6). Thus, we can assign the features at ~1170, 1120, and 1090 $cm^{-1}$ to stretching vibrations associated with the $C_2H_5$ groups, $\nu$(Si−O−C).[29,50,58] The small peak at ~990 $cm^{-1}$ may be attributed to stretching interactions of the Si−O bond.[15,81,82,84,85] Vibrational bands between ~1000 and 900 $cm^{-1}$ have been observed previously in mixed oxide silicates and are typically due to Si−O−M vibrations (where M represents a metal atom).[31,86] Although terminal Mo═O vibrations in $MoO_3$ are reported at ~995 $cm^{-1}$, we do not believe this feature is due to

a molybdenum oxide vibration since we do not observe a band at 880 $cm^{-1}$ (bulk oxide) and we have not observed any chemical shifts in the Mo(3d) XPS spectra indicative of oxide formation. The IRRAS spectrum in curve b, for the higher temperature TEOS deposition, is markedly different in shape than that shown in curve a. Here, the features due to $\nu$(Si−O−C) are significantly reduced, and a broad band at ∼1175 $cm^{-1}$ is observed. This spectrum is surprisingly similar to previously published IR spectra for $SiO_2$ thin films, fused quartz, and vitreous silica.[21,50,87−92] This indicates that the IR spectra are dominated by short-range order (which is dictated by Si−O chemical bonds), and therefore, the Si−O bond must be similar in all of these materials, even though the long-range structure may be somewhat different.[76,92] Specifically, in films of $SiO_2$ deposited via plasma-enhanced and TEOS CVD (∼4500 Å thick), features at ∼1177, 1090, and 1050 $cm^{-1}$ were attributed to Si−O vibrations;[29,50,88−92] hence, we assign the features at ∼1176, ∼1130, and ∼1050 $cm^{-1}$ in Figure 7A, curve b, accordingly. There is also a significant shoulder at ∼1210 $cm^{-1}$ in this spectra, which has been previously discussed in the literature in relation to IR spectra of $SiO_2$ thin films[50] and of vitreous silica.[87−89,93] This feature is more apparent in subtracted spectra presented below and will be discussed in more detail.

Several other interesting properties are revealed upon examination of Figure 7A. First, since the low-temperature IRRAS spectrum (Figure 7A, curve a) so clearly resembles the gas-phase TEOS spectrum (Figure 6), this provides additional evidence that the adsorbed species is an ethoxysilane intermediate when molybdenum is exposed to TEOS at low temperatures. Second, the absorption features show much greater intensity for the deposition conducted at 780 K as compared to the 380 K deposition. Furthermore, where the main peak in the 380 K spectrum represents a $\nu$(Si−O−C) vibration at ∼1120 $cm^{-1}$, the predominant feature in curve b is the broad band with features at ∼1176 and ∼1130 $cm^{-1}$. These latter peaks are representative of a $SiO_2$ thin film[58,87−89,91] and agree well with the XPS data (Figures 1 and 2A), which indicate that silicon dioxide is formed on Mo(100) surfaces upon initial exposure to TEOS at high temperature. Previously, Kirk has shown that the $AS_1$ and $AS_2$ modes (in-phase and out-of-phase motion of adjacent oxygen atoms, respectively) may show disorder-induced mechanical coupling that may broaden the primary $\nu$(Si−O) IR feature.[93]

Figure 7B shows the IRRAS spectra of TEOS-exposed Mo(100) surfaces after heating to ∼1000 K. Curve a represents the spectrum for a 380 K deposition and curve b for a 780 K deposition. Several changes occurred in the IRRAS spectra as a result of annealing. First, curve a shows significant intensity only at ∼1176, 1125, and ∼1030 $cm^{-1}$. These are similar peak positions to those observed for the as-dosed film at 780 K deposition (see Figure 7A, curve b) and in $SiO_2$ thin films.[50,87−89,91] Furthermore, the feature at ∼1090 $cm^{-1}$ is reduced to a small shoulder. The decrease in the absorption intensity of these features indicates loss of carbon since the $\nu$(Si−O−C) bands are reduced upon annealing. The changes in the IRRAS spectra upon heating for the higher deposition case are somewhat more subtle. Primarily, we observe a slight shift to higher wavenumber for the main $\nu$(Si−O) peaks and increased intensity at the 1210 $cm^{-1}$ shoulder (see Figure 7B, curve b). The fwhm of the primary feature in Figure 7B, curve b, is also slightly less than the as-dosed feature (Figure 7A, curve b), indicating that the $\nu$(Si−O) vibrations are better resolved as a result of the heat treatment. This behavior is

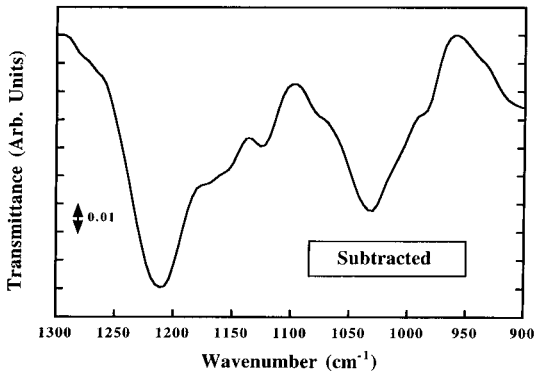


**Figure 8.** Subtracted IRRAS spectra of 780 K TEOS deposition after annealing.

in agreement with that reported previously for $SiO_2$ thin films (∼50 Å) formed by evaporating Si in an oxygen atmosphere on Mo(110) at room temperature[25] and from plasma-enhanced CVD of TEOS.[50] IRRAS spectra from those films showed a broad, asymmetric peak at ∼1178 $cm^{-1}$. A shift in the peak position of the $\nu$(Si−O) feature upon annealing was attributed to the improvement of order and stoichiometry in $SiO_2$ thin films.[25,50,58,76,81,85,88,93]

The changes in the $\nu$(Si−O) region are mirrored in the $\nu$-(C−H) region. Since the absorption for the latter vibrations is much weaker than the former,[94] we have not shown this portion of the IR spectra here. For deposition temperatures up to ∼600 K, we observe IR bands at ∼2980, 2930, and 2890 $cm^{-1}$. Previously, these vibrations have been assigned to C−H stretches in the $C_2H_5$ group of TEOS.[58,60,82,84,95,96] Upon heating the surfaces to ∼1000 K, we observe decreases in the $\nu$(C−H) absorption intensity; however, the IRRAS spectra of the heat-treated surfaces still show intensity in the $\nu$(C−H) region for Mo(100) surfaces exposed to TEOS at low temperatures. There are basically no features in the $\nu$(C−H) region for surfaces exposed at higher temperatures.

Figure 8 further demonstrates the changes in the $SiO_2$ film upon annealing. Here we show the subtracted spectrum for a film deposited at 780 K and annealed to ∼1000 K (Figure 7B, curve b), where the subtrahend is the IRRAS spectra for the as-dosed film (Figure 7A, curve b). The subtracted spectra thus shows the peaks that are introduced only as a function of annealing. The primary features observed in Figure 8 are peaks at ∼1210 $cm^{-1}$ and at ∼1030 $cm^{-1}$. Both of these features can be attributed to $\nu$(Si−O) bonds in films with some degree of structural order. We will discuss these features in greater detail in the next section.

## IV. Discussion

**A. Film Formation.** *1. $SiO_2$ Films at High Deposition Temperatures.* When TEOS is exposed to hot (≥700 K) Mo(100) surfaces, silicon dioxide formation results upon exposure. This is supported by our XPS, TPD, and IRRAS data. Figure 1A, curve b, shows the Si(2p) peak position indicative of $SiO_2$ with no change observed in the XPS spectra as the film is annealed (Figure 3A, curve b); and TPD shows no major reaction product desorption features (Figure 4, curves b). IRRAS peak positions and peak shapes shown in Figure 7A, curve b, are representative of IR spectra of fused quartz and vitreous silica.[50,87−89,93] Similarly, little change is noted in the IRRAS spectrum as a function of heating the surface (Figure 7B, curve b), except for slight peak shifts to higher frequency and small intensity increases in the $SiO_2$ features (shown in Figure 8).

All spectral features were assigned in Section III.C except the shoulder at ~1210 $cm^{-1}$, which requires further discussion. It is well-known for a film deposited on a conductive substrate with a thickness much less than the wavelength of the incident infrared radiation that the absorbance of transverse optical (TO) phonon modes are eliminated in single reflection spectroscopy, while the longitudinal optical (LO) modes show no change in absorbance as compared to transmission FTIR.[87,93] In the TO mode, the atomic displacement is perpendicular to the direction of periodicity of the elastic wave (the wave vector, **k**) while in longitudinal vibrations, the atomic displacement is parallel to the wave vector.[89,97] Thus, IRRAS probes LO modes preferentially vs transmission IR, which primarily probes TO modes.[93] Kirk has assigned asymmetric Si−O stretching modes in the IR spectral region from ~1300−900 $cm^{-1}$ and identified the in-phase ($AS_1$) and out-of-phase ($AS_2$) motions of adjacent oxygen atoms in fused quartz.[93] The $AS_2$ mode is generally weak in crystalline quartz, but in amorphous silica it typically increases in intensity at the expense of the intensity of the $AS_1$; thus, the relative intensities of these modes is an indication of crystallinity.[21,93] TO and LO splitting of the $AS_1$ and $AS_2$ modes have been observed in amorphous silica and the peaks have been assigned as LO($AS_1$) at 1256 $cm^{-1}$, LO($AS_2$) at 1160 $cm^{-1}$, TO($AS_1$) at 1076 $cm^{-1}$, and TO($AS_2$) at 1200 $cm^{-1}$[93]. This occurs because of *lack* of long-range order in amorphous films, which results in coupling of the $AS_1$ and $AS_2$ modes[21,89,93] such that all optical modes possess IR activity.[50] Although TO modes are typically not observed in reflection−absorption spectra, they may be observed in glasses and amorphous silica films that lack long-range crystallinity.[25,87,89,93] This is because in thin films, the *p*-polarized component of the IR radiation at oblique angles of incidence has subcomponents both parallel and perpendicular to the film surface, which can excite both LO and TO modes.[89,93] Thus, we attribute the feature at ~1210 $cm^{-1}$ in the subtracted spectrum of Figure 8 to the TO mode of the $AS_2$ vibration.[93] The observation of $AS_2$ vibrations in our IRRAS spectra provides evidence for a glasslike $SiO_2$ film as-deposited from TEOS pyrolysis on Mo(100).[21,89,93]

The small peak shifts in IRRAS spectra for high-temperature TEOS depositions account for an increase in the local structure of the $SiO_2$ films. Such an increase in film order is well-known to occur upon annealing $SiO_2$ films.[25,50,58,76,81,85,88,93] The primary reason for such improvements in the case of TEOS pyrolysis on Mo(100) at ≥700 K is likely due to the loss (upon heating) of a few $C_2H_5$ groups that may be incorporated in the film during the initial exposure. This is also indicated by comparing the C:Si atomic ratio shown in Figure 2A,B. A small amount of ethylene desorption occurs at ~850 K regardless of the TEOS deposition temperature, and it accounts for the decomposition products of these few, strongly adherent $C_2H_5$ groups. As for TEOS decomposition on Si(100), these ethyl groups may be further stabilized by the surface.[63] We observe the appearance of an IRRAS feature at ~1030 $cm^{-1}$ (Figure 8) upon annealing. This feature has been previously observed for more extensive {$SiO_4$} tetrahedral networks, and the appearance of this peak upon annealing the $SiO_2$ film further indicates some degree of order extending beyond a single {$SiO_4$} tetrahedral unit.[31,76,82] Heat treatment yielding IR peak shifts has been identified with densification of $SiO_2$ films formed by TEOS.[1,65] Densification is associated with improved electrical and mechanical properties such as porosity and strain, dry and wet etch rates, refractive index, and step coverage.[65]

Our spectroscopic evidence shows that TEOS deposition on Mo(100) at temperatures above ~700 K results in an amorphous or glassy-like film. Upon deposition of TEOS at *any* temperature, the sharp (1 × 1) LEED pattern that we routinely obtain for a clean Mo(100) surface was severely degraded. The background increased significantly, and no characteristic LEED spots were visible within the high background. Annealing reduced the background somewhat, but still no spots were visible. This verifies that although the local structure of the high-temperature films was improved by annealing, no *long-range*, three-dimensional, crystalline order exists in these films. This behavior has been reported previously for thin $SiO_2$ films on Mo(110) formed by Si evaporation in an oxygen atmosphere.[20,21,25,26] Thus, high-temperature pyrolysis of TEOS results in amorphous $SiO_2$ film with an extended network of {$SiO_4$} tetrahedra but with no long-range crystallinity.

*2. Reaction at Intermediate Temperatures.* At intermediate temperatures (~400−600 K), we observe different trends in film deposition and annealing than at the higher deposition temperatures. High-resolution XPS data of the Si(2p) region shows that with increasing deposition temperature, the binding energy gradually increases from ~102 to ~103 eV. This indicates a smooth transition with deposition temperature from adsorbed, molecular TEOS to the formation of $SiO_2$ upon exposure to a hot Mo(100) surface. This transition is probably accomplished by successive cleavage of ethoxy ligands from the central silicon atom of TEOS. This has been observed previously for TEOS on Si and amorphous $SiO_2$ surfaces.[2,59,60,64] Additionally, we believe that at temperatures between ~400 and 600 K, a species with stoichiometry of molecular TEOS adsorbs but is converted to an ethoxysilyl surface intermediate upon annealing to ~1000 K. The surface intermediate is probably in the form of a diethoxysilyl species. This is verified by the XPS data shown in Figure 2B, where upon annealing, the C:Si ratio is reduced to about 2, but the O:Si ratio remains at approximately 4. Normalized TPD data (Figure 5) show that roughly two $C_2$ groups are lost during the annealing process; this is consistent with decomposition of a molecular species to a diethoxysilyl intermediate. The final atomic ratios (Figure 2B) are also consistent with such a species, C:Si and O:Si ratios equal to 4 would be expected for a diethoxysilyl intermediate. Consistent with the apparent increase in the Si(2p) XPS signal after annealing (see Section II) is a model in which the geometry of the diethoxysilyl intermediate is such that the ethoxy groups point outward from the surface. For such a geometry, silicon atoms would be bound to the electron-rich Mo surface via two oxygen atoms. (Loss of oxygen during annealing is not observed to any significant extent, as indicated in Figure 2.). Formation of stoichiometric silicon dioxide thin films is not observed in this temperature range as a result of TEOS exposure to Mo(100).

However, at slightly higher temperatures (~600 and 700 K), primarily silicon dioxide is formed on the molybdenum surface during the initial exposure to TEOS, with contamination by monoethoxysilyl ligands decreasing with increasing deposition temperature. This is indicated by the Si(2p) binding energy and the IRRAS peak positions and peaks shapes in the 1300−900 $cm^{-1}$ region. It is known that for TEOS decomposition at and above these temperatures, the rate of intermediate formation is much less than the deposition rate of $SiO_2$,[8] and in this temperature regime, the substrate possesses enough energy to cleave two or more C−O bonds (~360 kJ/mol) in the TEOS molecule during deposition.[9] Since these temperatures are too high for ethylene and ethanol to remain on the surface, these reaction products immediately desorb to the gas phase. However, the temperature is not high enough to remove all of the

ethoxy ligands, and the growing film is contaminated with a monoethoxysilyl species. The C:Si and O:Si atomic ratios shown in Figure 2 are consistent with this stoichiometry. The IRRAS spectra are also congruous with this interpretation. The $\nu$(Si−O−C) features are strong in the intermediate temperature range but decrease in intensity with increasing deposition temperature. The spectra undergo a smooth transition from distinct peaks at ∼1170 and 1120 $cm^{-1}$ (Figure 7A, curve a) to the broad $\nu$(Si−O) feature at ∼1175 $cm^{-1}$ (Figure 7A, curve b). Similarly, after annealing the IRRAS spectra undergo a smooth transition as a function of deposition temperature where the spectra at low deposition temperatures are represented by curve a in Figure 7B, and those at higher temperatures by those in curve b in Figure 7B. Furthermore, after the heat treatment, all of the spectra show decreased absorption intensity at ∼1120 $cm^{-1}$, and a resulting broad feature with strong intensity at ∼1175 $cm^{-1}$. This indicates that, with increasing deposition temperature, less Si−O−C bonds remain on the surface and isolated $\nu$(Si−O) vibrations are observed to a greater extent. So with increasing deposition temperature, the as-dosed IRRAS spectrum gradually shifts from one nearly identical to gas-phase TEOS to one that is nearly identical to fused quartz or vitreous silica.[87−89,93] The TO mode peak at 1210 $cm^{-1}$ is clearly resolved at ∼700 K in subtracted spectra (as in Figure 8). The absence of this feature shows that $SiO_2$ with some degree of structural order is not formed in this intermediate temperature range.

*3. Deposition of TEOS Near Room Temperature.* When TEOS is exposed to the clean Mo(100) single-crystal surface near room temperature, only small amounts adsorb, indicating that the room-temperature sticking coefficient is low. However, since the normalized Si(2p), O(1s), and C(1s) signals are significantly larger at higher deposition temperatures, we can conclude that the reactive sticking coefficient for TEOS is much greater at elevated temperatures. Adsorption near room temperature is molecular, as indicated by the sharp desorption features for $m/e = 26$ and 31 (not shown), as well as the atomic O:Si, C:Si, and C:O ratios calculated from XPS data (Figure 2). These ratios are (within the error bars of the XPS sensitivity factors) approximately 4, 8, and 2: the ratios expected for molecular TEOS. In addition, the IRRAS spectrum is nearly identical to the gas-phase molecular TEOS IR transmission spectrum (Figure 6). The peak position of the Si(2p) feature at ∼102 eV (Figure 1A, curve a) is indicative of Si bound tetrahedrally to four oxygen atoms and is representative of a silicate or alkoxysilane chemical environment.[20,22,35] Although we observe some changes in the XPS and IRRAS spectra as a function of annealing (Figures 3 and 7), formation of stoichiometric silicon dioxide is not achieved for room-temperature TEOS exposure. For example, the Si(2p) binding energy in Figure 3A, curve a, is not significantly different than that of the as-dosed surface (Figure 1A). This indicates that no significant change in the chemical environment has occurred upon heating and that silicon is still bound as an alkoxysilane. Furthermore, the O:Si, C:Si, and C:O ratios remain at values of approximately 4, 8, and 2, which are expected for undissociated TEOS. Though we note intensity decreases in the $\nu$(Si−O−C) feature at ∼1090 $cm^{-1}$ and the Si−O−Mo vibrational feature at ∼995 $cm^{-1}$, the $\nu$(Si−O−C) feature is not eliminated and the features typically associated with $SiO_2$ thin films (as in Figure 8) are not introduced to any significant extent. Thus, we conclude for a room-temperature deposition on Mo(100), TEOS adsorbs primarily in a molecular fashion, and some can be desorbed to the gas phase by heating. Figures 1C and 3C demonstrate that surface carbon, as well, changes little as a function of annealing and remains on the surface in the form of ethoxide groups, most likely bound to Si, as indicated by the IRRAS data. That the ethoxy groups remain after the high-temperature annealing cycle may be somewhat surprising. However, we do not believe that the Si−O−C bond has been broken, since the IRRAS data clearly show vibrational features at ∼1090 $cm^{-1}$. Further, a shift of about −0.5 eV in the $Mo(3d)_{5/2}$ peak would be expected if the ethoxy bonds had cleaved and a metal carbide species had formed on the surface.[98,99] A surface layer of $SiO_x$−C has been reported for flame pyrolysis on Ag−Pd−Cu alloys at a temperature of ∼400 K,[100] and partially pyrolyzed TEOS has been observed on graphite surfaces for temperatures as high as 750 K.[101]

In summary, TEOS adsorbs molecularly at room temperature. As the deposition temperature increases, the number of ethoxy ligands on the molecule decrease, and at the highest deposition temperatures examined in this study, silicon dioxide is formed upon exposure. Annealing these surfaces can result in a decrease in the number of ethoxy groups for surfaces exposed to TEOS at intermediate temperatures, while heat treatment of the $SiO_2$ films results in somewhat better long-range order, probably in the form of extended $\{SiO_4\}$ tetrahedral networks.

**B. Exposure.** To determine the rate-limiting step of $SiO_2$ formation by TEOS decomposition, we studied XPS and TPD as a function of exposure time. For a TEOS pressure of $\sim 4 \times 10^{-7}$ Torr, at a sample temperature of 700 K, we varied the exposure time from 5 to 30 min. (Recall that our standard exposure was 15 min; all other experimental parameters were as given in Section II.) As discussed above, TEOS pyrolysis at 700 K results in $SiO_2$ film formation upon exposure, with relatively little carbon contamination. For exposure between 5 and 30 min exposure times, we observe a deviation in the normalized Si(2p) peak intensity of only ±7% from the standard exposure (15 min). Although the exposure time was varied by a factor of 6, only negligible changes in the Si(2p) XPS peak intensity were observed, with no change in peak position. A similar bandwidth of ±7% is observed after annealing. In fact, the absolute peak intensity of peak $\gamma$ in the TPD spectra is nearly identical for these exposures. This indicates that TEOS reacting to form $SiO_2$ is not limited by the exposure time but is surface reaction limited. It is probable that the limiting step is associated with C−O bond cleavage in the precursor species.[8,9]

Reaction-limited $SiO_2$ formation on thick silicon dioxide layers by decomposition of TEOS has been reported for low-pressure, hot- and cold-wall CVD reactors, and the kinetics of the reaction over a variety of pressure and temperature ranges have also been reported.[1,8,9,13] These mechanisms have been reviewed recently by Cale and Mahadev.[102] The CVD reactor data indicates that $SiO_2$ film growth at low pressures (0.1−1 Torr) depends both on the number of precursor molecules impinging upon the substrate and on the surface lifetime of the decomposition products.[1,102] It has been speculated that surface reactivity is also inhibited by decomposition products, such as ethylene, remaining on the surface.[1,8,9,13] Becker et al. attempted to increase the growth rate by increasing the TEOS pressure (in order to increase the flux to the surface) and found no change since an increase in precursor pressure did not change the desorption rate of reaction byproducts.[1]

In cold-wall CVD reactors, which our chamber most closely models, the reaction is known to be heterogeneous and the rate-limiting step is TEOS decomposition.[13,103,104] The most widely accepted model involves a heterogeneous decomposition mech-

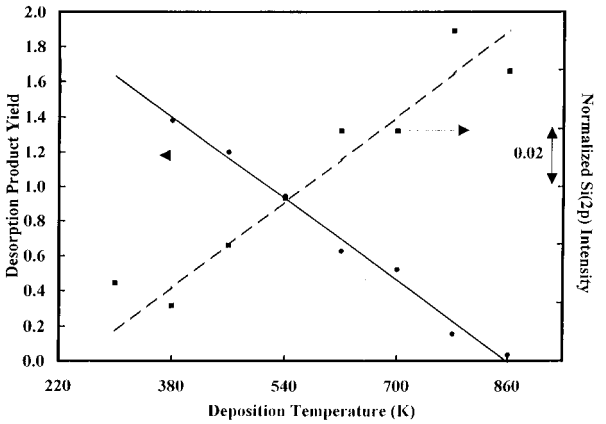


**Figure 9.** Total $C_2$ desorption product yield for TEOS depositions above room temperature (left axis, ●, solid line) and the normalized Si(2p) XPS intensity (right axis, ■, dashed line) as a function of TEOS deposition temperature.

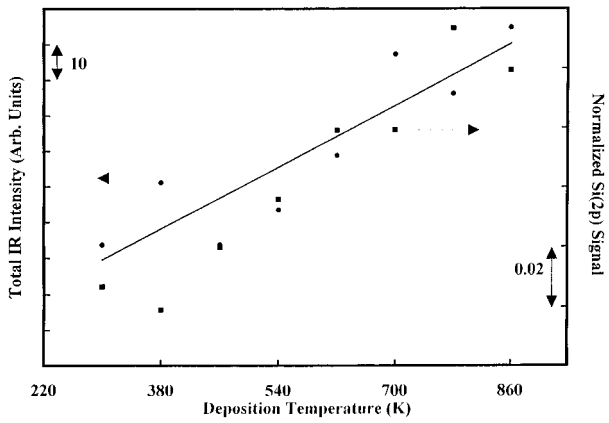


**Figure 10.** Total IRRAS intensity in the $\nu$(Si−O) region (∼1300−900 $cm^{-1}$) on the left axis (●) and the normalized Si(2p) XPS intensity on the right axis (■) as a function of TEOS deposition temperature.

anism involving adsorbed TEOS.[102] The gaseous byproducts formed by the deposition reaction can readsorb on the growing film surface, inhibiting deposition. Assuming the initial decomposition step is rate-limiting and that all adsorption steps are in equilibrium leads to a model that is in excellent agreement with conformality measurements. This model yields first-order dependence in TEOS concentration at low conversion. Bartram et al. have recently reported values of the TEOS reaction order and the reactive sticking coefficient[103,104] of unity and $6 \times 10^{-7}$, respectively. In addition, their measurements provide compelling evidence that byproduct inhibition does not effect the heterogeneous reaction rate under normal CVD conditions.[104] Although our deposition measurements are on a bare metal surface at substantially lower temperature, our XPS and TPD data from exposure time measurements agree well with these prior studies. For exposure times between 5 and 30 min, the $SiO_2$ film that is formed shows no difference in film thickness (as indicated by a lack of changes in the Si(2p) intensity) and no difference in intermediate and/or product chemistry (as indicated by the quantitatively identical decomposition products observed in TPD). Thus, our data indicate that TEOS decomposition resulting in ultrathin $SiO_2$ film formation at temperatures between 700 and 860 K is reaction-limited by one or more surface processes. For example, it is possible that the surface reactive sites are saturated within the first 5 min of exposure such that no more TEOS can decompose on the surface. However, our data would also support a model of product inhibition that would limit the amount of precursor that can decompose at a given temperature since ethylene is still present on the surface at 850 K even for a deposition temperature as high as 780 K (Figure 4A). Therefore, we cannot distinguish between the two mechanisms from our data.

TPD and XPS data supporting reaction-limited TEOS decomposition on Mo(100) is presented in Figure 9. We show the total desorption product yield (neglecting TPD data for the room-temperature exposure that did not result in any $SiO_2$ formation) and the normalized Si(2p) peak intensity as a function of deposition temperature. Recall (Section IIIB) that the primary desorption product is ethylene. Increases in the Si(2p) peak intensity have previously been shown to correlate linearly with $SiO_2$ film thickness on Si(100) surfaces.[61] Similarly, if we take the Si(2p) peak intensity to be a measure of film thickness/continuity (see below), it is obvious that as the deposition temperature increases, a thicker film is formed with fewer decomposition products desorbing to the gas phase. Comparing the normalized Si(2p) peak intensity across the temperature range studied, we can further conclude that the reactivity of TEOS at low temperatures is very low which is in agreement with other studies.[103,104] These data supports a mechanism where TEOS decomposition is reaction-limited and where the surface reactivity for $SiO_2$ formation could be inhibited with byproduct formation (ethylene).

**C. Film Thickness.** Figure 10 shows the total integrated peak intensity in the 1300−900 $cm^{-1}$ region and the normalized Si(2p) signal intensity as a function of TEOS deposition temperature. This demonstrates that the peak intensity in the $\nu$(Si−O) region increases approximately linearly as a function of deposition temperature. Previous studies have demonstrated that the IR peak intensity in the $\nu$(Si−O) region varies linearly with the thickness of thermally grown silicon dioxide films[91] and of films deposited by photochemical CVD.[62] The latter case showed the total integrated IR absorption in the asymmetrical stretching region (∼1300−900 $cm^{-1}$) correlated linearly with the integrated area of the Si(2p) peak, and the authors were able to extract film thickness data from IR data.[62] Thus, the total IR intensity in the 1300−900 $cm^{-1}$ region is a measure of the $SiO_2$ film thickness due to the higher density of absorbing Si−O bonds.[91] Since the $\nu$(Si−O) IR peak intensity increases with deposition temperature (Figure 10), we can conclude that a greater number of absorbing Si−O bonds are present in films deposited at higher temperatures, and therefore, thicker/more continuous films are formed. The total IR peak intensity as a function of deposition temperature also is linearly related to the XPS data (Figure 10); this indicates that as the Si(2p) peak intensity increases, the film thickness is increasing as would be expected. These data also agree well with $SiO_2$ formation by TEOS pyrolysis on other molybdenum surfaces (foil and wire) at temperatures between 1000 and 1600 K, where film thickness was also observed to increase as a function of deposition temperature.[12,13] However, in the lower temperature regime, the films may not be continuous, and a film thickness correlation based solely on Figure 10 must be done with some care.

We have also estimated film coverages based on angle-resolved XPS spectra (ARXPS). In this technique, the takeoff angle is varied, such that at higher angles, the electron escape depth is small and XPS samples the near-surface region only, while a takeoff angle near normal (0°) shows greater signal contributions from the bulk. Thus, we have compared our normalized Si(2p) and O(1s) XPS signals at different takeoff angles to those expected theoretically,[55] where, for our experiment, the adjustable parameters are film thickness and the fraction of the surface covered. This comparison yields a film

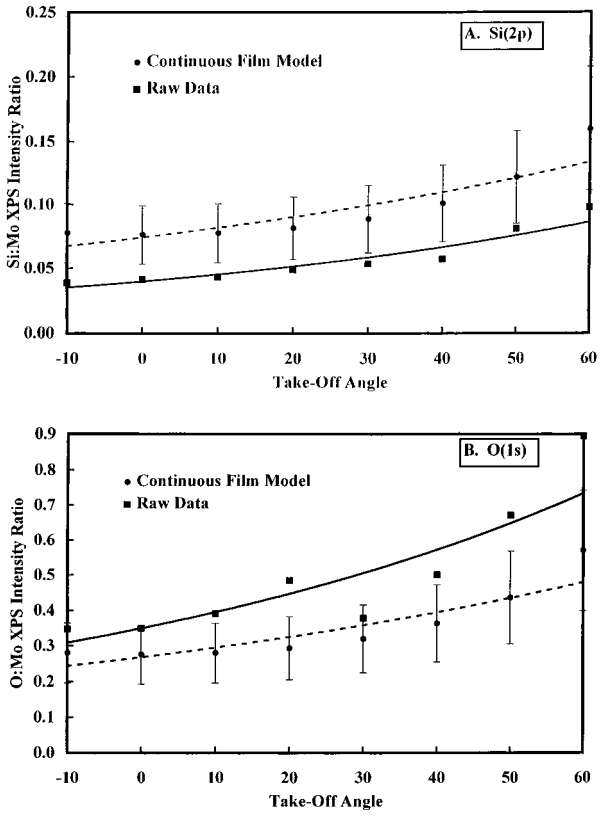


**Figure 11.** ARXPS data for Si:Mo (A) and O:Mo (B) as a function of takeoff angle (■) and a continuous film model (●). TEOS deposition was at 860 K, resulting in $SiO_2$ formation (see text). The error bars are ±30% for the model data.

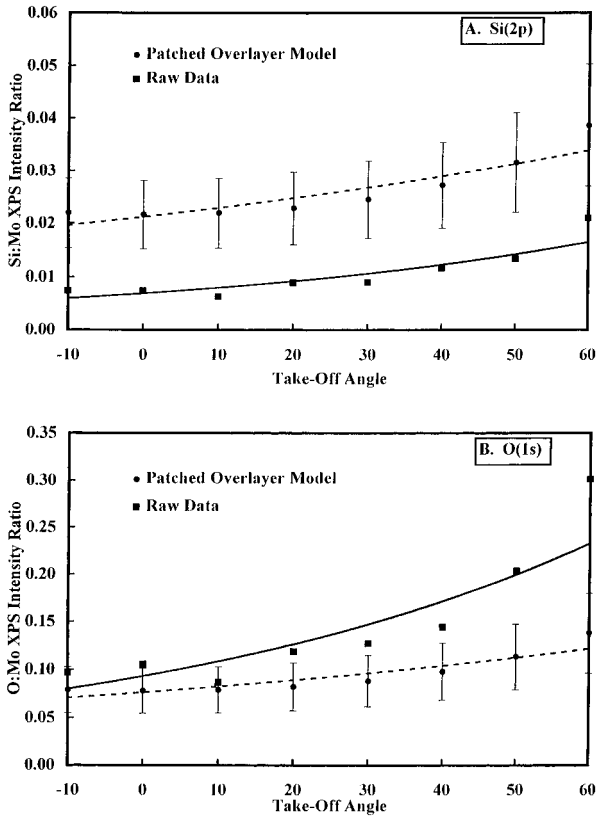


**Figure 12.** ARXPS data for Si:Mo (A) and O:Mo (B) as a function of takeoff angle (■) and a patched overlayer model (●). TEOS deposition was at 380 K, resulting in the formation of a diethoxysilyl intermediate (see text). The error bars are ±30% for the model data.

thickness of roughly a monolayer at 860 K with the entire surface covered by $SiO_2$, while at the lower deposition temperature, only 25% of the surface is covered.

*1. ARXPS of $SiO_2$ Film by TEOS Pyrolysis at 860 K.* Parts A and B of Figure 11 show the Si(2p) and O(1s) ARXPS data, respectively, for a $SiO_2$ film deposited by TEOS pyrolysis at 860 K. The raw Si(2p):Mo(3d)$_{5/2}$ data is plotted in Figure 11A as a function of takeoff angle and is shown with predictions calculated using a continuous film model, as shown in eq 5:[55]

$$\frac{I_{Si}}{I_{Mo}} = \left(\frac{I^{\infty}_{Si}}{I^{\infty}_{Mo}}\right)\left[1 - \exp\left(\frac{-t}{\lambda_{Si}\sin(90-\theta)}\right)\right] \times \left[\exp\left(\frac{t}{\lambda_{Mo}\sin(90-\theta)}\right)\right] \quad (5)$$

Here, $t$ is the film thickness in nm; $\lambda_x$ is the escape depth of the respective photoelectron through an inorganic layer, defined as the IMFP as above (Section II); and $\theta$ is the takeoff angle. The first term in eq 5 represents the Si(2p):Mo(3d)$_{5/2}$ intensity ratio for infinitely thick layers of $SiO_2$ and Mo metal, respectively. As we showed in the previous subsection, $SiO_2$ film formation is reaction-limited, such that the film thickness for a given deposition temperature is fixed. Thus, we have estimated the first term in eq 5 by the ratio of the theoretical sensitivity factors, given by eq 3, above:

$$\frac{I^{\infty}_{Si}}{I^{\infty}_{Mo}} \approx \frac{S_{Si}}{S_{Mo}} \quad (6)$$

Although this estimate may introduce systematic error to the absolute film thickness calculation, the experimental trend in the raw ARXPS data shown in Figure 11 demonstrates good qualitative agreement with theory. (Data shown in Figure 11B for the continuous model use eq 5 with the sensitivity and IMFP for O(1s) substituted appropriately.) In Figure 11, we have assumed a thickness of 2.5 Å for the model, which is in agreement with the raw data within the limitations of our calculations. (The most significant contribution to the deviation between the model and our raw data is a systematic error that may be introduced by eq 6, and errors associated with the calculation of the IMFP and *T(E)*, as discussed in Section II; we show error bars of ±30% in Figure 11A,B.) This thickness provided the best fit to both the normalized Si(2p) and the normalized O(1s) data. Since the Si(2p) signal is typically small and the noise level is higher for this signal than for the O(1s) signal, the model overestimates the Si:Mo intensity ratio, while it underestimates the O:Mo intensity ratio. A thickness of 2.5 Å is not unreasonable on the basis of a simple calculation using known bond lengths; the Si−O bond length is ∼1.5 Å and the Mo−O bond is ∼2 Å for molybdenum oxide compounds.[105,106] Such a geometry is feasible if silicon dioxide bonds to the electron-rich molybdenum surface via Mo−O bonds. Therefore, we estimate the coverage of $SiO_2$ on Mo(100) by TEOS pyrolysis at 860 K to be one monolayer on the basis of these calculations.

*2. ARXPS of Ethoxysilane Film at 380 K.* Parts A and B of Figure 12 show the normalized Si(2p) and O(1s) XPS intensities as a function of takeoff angle, respectively, and model ARXPS calculations for TEOS deposited on Mo(100) at 380 K. Recall that at this temperature a diethoxysilyl surface species is formed on the surface (see above). In Figure 12 A, we have compared the raw data to a model in which the surface is covered with an attenuating but patched overlayer, according to Fadley:[55]

$$\frac{I_{Si}}{I_{Mo}} = \frac{\left(\frac{I^{\infty}_{Si}}{I^{\infty}_{Mo}}\right)\gamma \exp\left(\frac{-t}{\lambda_{Si}\sin(90-\theta)}\right)}{\left[(I-\gamma)+\gamma\exp\left(\frac{-t}{\lambda_{Mo}\sin(90-\theta)}\right)\right]} \quad (7)$$

In this model, all of the terms are defined as in eqs 5 and 6; $\gamma$ represents the fraction of the surface covered by the overlayer. (Appropriate substitutions of the IMFP and sensitivity factor are made for the O(1s) calculations shown in Figure 12B.) In Figure 12, the adjustable parameters, $t$ and $\gamma$, are assigned values of 2.5 Å and 0.25, representing a monolayer (as discussed above) that covers ∼25% of the Mo(100) surface. As shown above, Figure 12 demonstrates that the model overestimates the Si:Mo ratio while underestimating the O:Mo ratio. Again, this systematic error is likely introduced by the estimation involved in eq 6 and the parameters used to calculate the sensitivity factors; thus a ±30% error is allowed for the model. It is important to note, however, that the model qualitatively represents the experimental data, and when the continuous film model is applied to these experimental data, there is no agreement. (In fact, for the model to fit the data within a factor of 2, the thickness of a continuous, attenuating overlayer was calculated to be less than 0.1 Å, which is not physically possible based upon our XPS, TPD, and IRRAS data.) In addition, the percent coverage estimated by a patched overlayer model is reasonable if we simply assume that each diethoxysilyl intermediate blocks approximately 3−4 Mo sites. Site-blocking could also account for the increased dissociation of TEOS as a function of deposition temperature if electron-rich surface sites are inaccessible to the ethoxysilyl intermediate, by adsorption of other intermediates or decomposition products (see above). Occupation of active surface sites would then hinder further TEOS and/or ethoxysilyl intermediate decomposition. The percent coverage illustrated in Figure 12A,B is further warranted if we compare the bond lengths of molybdenum and of ethoxy chains bound to silicon. By simple geometry, if we assume that the ethoxy chain is linear and not parallel to the Mo(100) surface, we find that each diethoxysilyl intermediate can block four nearest-neighbor sites. This is in agreement with the surface coverage calculated by the patched overlayer model for our ARXPS data, as shown in Figure 12A,B. In this case, we do not expect the surface geometry of the Si and O atoms to be significantly different for the ethoxysilyl intermediate as compared to $\{SiO_4\}$ tetrahedra in stoichiometric silicon dioxide.

In Figure 13 we show the Si(2p) XPS signal intensity as a function of deposition temperature and the linearization of Figure 10 on the left axis. On the right axis, we show a surface coverage (%) where we assume a monolayer of $SiO_2$ is formed for TEOS deposition on Mo(100) at 860 K, as indicated by ARXPS in Figure 11. The surface coverage is as low as ∼12% for TEOS deposition at room temperature, which is in agreement with XPS results (see Figure 1, curves a) suggesting the sticking coefficient of TEOS near room temperature is quite low. Additionally, above deposition temperatures of ∼600 K, stoichiometric $SiO_2$ is formed during TEOS deposition with at least 75% of the surface covered. At higher temperatures, the silica film is uniform. These data is in good agreement with prior studies showing that silicon dioxide films formed by TEOS pyrolysis yield good step coverage.[1,14,65]

## V. Summary

In this paper, we have demonstrated that monolayer $SiO_2$ films can be grown on a single-crystal transition metal surface with little carbon contamination and with the many benefits of a single-source precursor. No high-temperature heat treatment is necessary as the films deposited by TEOS pyrolysis at temperatures greater than about 700 K demonstrate XPS and IRRAS features expected for stoichiometric $SiO_2$. Annealing these films, however, yields enhanced film order as indicated by peak shifts in the IR spectra. The reactivity of the Mo(100) surface for TEOS decomposition is surprisingly low, even lower that the reactivity on metal oxide surfaces,[49,58,107] as evidenced by the low sticking probability.

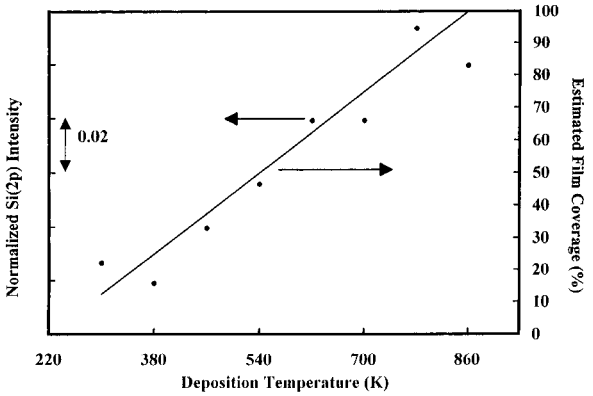


**Figure 13.** Normalized Si(2p) XPS intensity (●, left axis) as a function of deposition temperature. The solid line (right axis) represents a linear fit to ARXPS film coverage data (see text).

At lower deposition temperatures, a diethoxysilyl intermediate is formed by exposure of Mo(100) to TEOS, and upon annealing, ethoxy groups are cleaved to produce gas-phase ethylene. Stoichiometric *and* continuous silicon dioxide is not formed at these low temperatures. However, at higher deposition temperatures the films are stoichiometric $SiO_2$, and we have shown that the surface coverage is linearly correlated to the normalized Si(2p) XPS intensity and to the $\nu$(Si−O) IRRAS peak areas. These correlations will prove useful for estimating film thickness and coverage for future investigations of ultrathin silicon dioxide films.

**Acknowledgment.** The authors gratefully acknowledge support under NSF Grant CTS-9303974 and from Battelle Pacific Northwest National Laboratories. T.A.J.-K. would also like to express sincere appreciation to the Intel Foundation for financial support during the completion of this work.

## References and Notes

(1) Becker, F. S.; Pwlik, D.; Anzinger, H.; Spitzer, A. *J. Vac. Sci. Technol. B* **1987**, *5*, 1555−1563.
(2) Crowell, J. E.; Tedder, L. L.; Cho, H.-C.; Cascarano, F. M.; Logan, M. A. *J. Vac. Sci. Technol. A* **1990**, *8*, 1864−1870.
(3) Jin, T.; Jo, S. K.; Yoon, C.; White, J. M. *Chem. Mater.* **1989**, *1*, 308−311.
(4) Danner, J. B.; Vohs, J. M. *Appl. Surf. Sci.* **1993**, *72*, 409−417.
(5) Adams, A. C.; Capio, C. D. *J. Electrochem. Soc.* **1979**, *126*, 1042−1046.
(6) Becker, F. S.; Rohl, S. *J. Electrochem. Soc.* **1987**, *134*, 2923−2931.
(7) Levy, T. A.; Gallagher, P. K.; Schrey, F. *J. Electrochem. Soc.* **1987**, *132*, 430−437.
(8) Desu, S. B. *J. Am. Ceram. Soc.* **1989**, *72*, 1615−1621.
(9) Kalidinidi, S. R.; Desu, S. B. *J. Electrochem. Soc.* **1990**, *137*, 624−628.
(10) Emesh, I. T.; D'Asti, G.; Mercier, J. S.; Leung, P. *J. Electrochem. Soc.* **1989**, *136*, 3404−3408.
(11) Pai, C. S.; Miner, J. F.; Foo, P. D. *J. Electrochem. Soc.* **1992**, *139*, 850−856.
(12) Tiller, H.-J.; Weinke, J.; Meyer, J. *J. Electrochem. Soc.* **1994**, *141*, 514−518.
(13) Haupfear, E. A.; Olson, E. C.; Schmidt, L. D. *J. Electrochem. Soc.* **1994**, *141*, 1943−1950.

(14) Ong, T. P.; Tobin, P.; Mele, T. *J. Appl. Phys.* **1995**, *77*, 6055−6057.
(15) Kurth, D. G.; Bein, T. *J. Phys. Chem.* **1992**, *96*, 6707−6712.
(16) Okuhara, T.; White, J. M. *Appl. Surf. Sci.* **1987**, *29*, 223−241.
(17) Brinker, C. J.; Harrington, M. S. *Sol. Energy Mater.* **1981**, *5*, 159−172.
(18) Brinker, C. J.; Bunker, B. C.; Tallant, D. R.; Ward, K. J. *J. Chim. Phys.* **1986**, *83*, 851−858.
(19) Wachtman, J. B.; Haber, R. A. Ceramic Films and Coatings−Overview. In *Ceramic Films and Coatings*; Wachtman, J. B., Haber, R. A., Eds.; Noyes Publications: Park Ridge, NJ, 1993.
(20) He, J.-W.; Xu, X.; Corneille, J. S.; Goodman, D. W. *Surf. Sci.* **1992**, *279*, 119−126.
(21) Xu, X.; Goodman, D. W. *Surf. Sci.* **1993**, *282*, 323−332.
(22) Sarrazin, P.; Kasztelan, S.; Zanier-Szdlowski, N.; Bonnelle, J. P.; Grimblot, J. *J. Phys. Chem.* **1993**, *97*, 5947−5953.
(23) Rodrigo, L.; Adnot, A.; Roberge, P. C.; Kaliaguine, S. *J. Catal.* **1987**, *105*, 175−186.
(24) Li, C.; Xin, Q.; Wang, K.-L.; Guo, X. *Appl. Spectrosc.* **1991**, *45*, 874−882.
(25) Xu, X.; Goodman, D. W. *Appl. Phys. Lett.* **1992**, *61*, 774−776.
(26) Grudling, C.; Lercher, J. A.; Goodman, D. W. *Surf. Sci.* **1994**, *318*, 97−103.
(27) Stencel, J. M.; Diehl, J. R.; D'Este, J. R.; Makovsky, L. E.; Rodrigo, L.; Marcinkowska, K.; Adnot, A.; Roberge, P. C.; Kaliaguine, S. *J. Phys. Chem.* **1986**, *90*, 4739−4743.
(28) Gajardo, P.; Pirotte, D.; Defosse, C.; Grange, P.; Delmon, B. *J. Electron Spectrosc. Relat. Phenom.* **1979**, *17*, 121−135.
(29) Takeuchi, H.; Izumi, H.; Kawasaki, A. Decomposition Study of TEOS in Thermal CVD. *Mater. Res. Soc. Symp. Proc.* Boston, MA; 1994.
(30) Liu, H.; Bertolet, D. C.; Rogers, J. W., Jr. *Surf. Sci.* **1994**, *320*, 145−160.
(31) Smith, A. L. *Spectrochim. Acta* **1960**, *16*, 87−105.
(32) Charles, C.; Garcia, P.; Grolleau, B.; Turban, G. *J. Vac. Sci. Technol. A* **1992**, *10*, 1407−1413.
(33) *The Wiley/NBS Registry of Mass Spectral Data*; McLafferty, F. W., Stauffer, D. B., Eds.; Wiley-Interscience: New York, 1989.
(34) *Eight Peak Index of Mass Spectra*, 3 ed.; The Royal Society of Chemistry: Herts, U.K., 1983.
(35) *Handbook of X.-Ray Photoelectron Spectroscopy*; Wagner, C. D.; Riggs, W. M.; Davis, L. E.; Moulder, J. F.; Muilenberg, G. E., Eds.; Perkin-Elmer Corp.: Eden Prairie, MN, 1979.
(36) Brox, B.; Olefjord, I. *Surf. Interface Anal.* **1988**, *13*, 3−6.
(37) Flaim, T. A.; Ownby, P. D. *J. Vac. Sci. Technol.* **1973**, *3*, 661−662.
(38) Urban, M. W.; Koenig, J. L. Recent Developments in Depth Profiling from Surfaces Using FTIR Spectroscopy. In *Vibration Spectra and Structure*; During, J. R., Ed.; Elsevier: Amsterdam, 1990.
(39) Bermudez, V. M.; Prokes, S. M. *Surf. Sci.* **1991**, *248*, 201−206.
(40) Finke, S. J.; Schrader, G. L. *Spectrochim. Acta* **1990**, *46A*, 91−96.
(41) Bermudez, V. M. *J. Phys. Chem.* **1994**, *98*, 2469−2477.
(42) Greenler, R. G. *J. Vac. Sci. Technol.* **1975**, *12*, 1410−1417.
(43) Hoffman, F. M. *Surf. Sci. Rep.* **1983**, *3*, 107−192.
(44) Gopel, W. *Surf. Sci. Rep.* **1985**, *20*, 9−103.
(45) Chabal, Y. J. *Surf. Sci. Rep.* **1988**, *8*, 211−357.
(46) Nafie, L. A. Polarization Modulation FTIR Spectroscopy. In *Advances in Applied Fourier Transform Infrared Spectroscopy*; Mackenzie, M. W., Ed.; Wiley: New York, 1988.
(47) Bermudez, V. M. *J. Appl. Phys.* **1992**, *71*, 5450−5459.
(48) Shirley, D. A. *Phys. Rev. B* **1972**, *5*, 4709−4714.
(49) Gamble, L.; Hugenschmidt, M. B.; Campbell, C. T.; Jurgens, T. A.; Rogers, J. W., Jr. *J. Am. Chem. Soc.* **1993**, *115*, 12096−12105.
(50) Goullet, A.; Charles, C.; Garcia, P.; Turban, G. *J. Appl. Phys.* **1993**, *74*, 6876−6882.
(51) Kim, K. S.; Barteau, M. A. *J. Mol. Catal.* **1990**, *63*, 103−117.
(52) Bakke, A. A.; Chen, H.-W.; Jolly, W. L. *J. Electron Spectrosc. Relat. Phenom.* **1980**, *20*, 333−366.
(53) Wagner, C. D.; Davis, L. E.; Zeller, M. V.; Taylor, J. A.; Raymond, R. H.; Gale, L. H. *Surf. Interface Anal.* **1981**, *3*, 211−225.
(54) Smith, G. C. *Surface Analysis by Electron Spectroscopy: Measurement and Interpretation*; Plenum Press: New York, 1994.
(55) Fadley, C. S. *Prog. Surf. Sci.* **1984**, *16*, 275−388.
(56) Seah, M. P.; Dench, W. A. *Surf. Interface Anal.* **1979**, *1*, 2−11.
(57) Yeh, J. J.; Lindau, I. *At. Nucl. Data Tab.* **1985**, *32*, 1−155.
(58) Jurgens, T. A.; Rogers, J. W., Jr. *J. Phys. Chem.* **1995**, *99*, 731−743.
(59) Tedder, L. L.; Crowell, J. E.; Logan, M. A. *J. Vac. Sci. Technol. A* **1991**, *9*, 1002−1006.
(60) Tedder, L. L.; Lu, G.; Crowell, J. E. *J. Appl. Phys.* **1991**, *69*, 7037−7049.
(61) Danner, J. B.; Vohs, J. M. *Langmuir* **1994**, *10*, 3116−3121.
(62) Licoppe, C.; Meriadec, C.; Nissim, Y. I.; Moison, J. M. *Appl. Surf. Sci.* **1992**, *54*, 445−452.
(63) Danner, J. B.; Reuter, M. A.; Vohs, J. M. *Langmuir* **1993**, *9*, 455−459.
(64) Crowell, J. E.; Tedder, L. L.; Cho, H.-C.; Cascarano, F. M.; Logan, M. A. *J. Electron Spectrosc. Relat. Phenom.* **1990**, *54/55*, 1097−1104.
(65) Pliskin, W. A. *J. Vac. Sci. Technol.* **1977**, *14*, 1064−1081.
(66) Wang, L.; Tysoe, W. T. *Surf. Sci.* **1990**, *236*, 325−340.
(67) Miles, S. L.; Bernasek, S. L.; Gland, J. L. *J. Electron Spectrosc. Relat. Phenom.* **1983**, *29*, 239−246.
(68) Ohuchi, F.; Firment, L. E.; Chowdhry, U.; Ferretti, A. *J. Vac. Sci. Technol. A* **1984**, *2*, 1022−1023.
(69) Henry, R. M.; Walker, B. W.; Stair, P. C. *Surf. Sci.* **1985**, *155*, 732−750.
(70) Kurtz, R. L.; Stockbauer, R.; Madey, T. E.; Roman, E.; de Segovia, J. L. *Surf. Sci.* **1989**, *218*, 178−200.
(71) Chen, J. G.; Colianni, M. L.; Weinberg, W. H.; Yates, J. T., Jr. *Chem. Phys. Lett.* **1991**, *177*, 113−117.
(72) Zaera, F.; Kollin, E.; Gland, J. L. *Chem. Phys. Lett.* **1985**, *121*, 464−468.
(73) He, J.-W.; Kuhn, W. K.; Goodman, D. W. *Surf. Sci.* **1992**, *262*, 351−358.
(74) Fukui, K.; Aruga, T.; Iwasawa, Y. *Surf. Sci.* **1993**, *281*, 241−252.
(75) Ko, E. I.; Madix, R. J. *Surf. Sci.* **1981**, *109*, 221−238.
(76) Sen, P. N.; Thorpe, M. F. *Phys. Rev. B* **1977**, *15*, 4030−4038.
(77) Silverstein, R. M.; Bassler, G. C.; Morrill, T. C. *Spectrometric Identification of Organic Compounds*, 4th ed.; John Wiley and Sons: Toronto, 1981.
(78) Gaboury, S. R.; Urban, M. W. *Polym. Prepr.* **1988**, *29*, 356−357.
(79) Simon, I.; McMahon, H. O. *J. Chem. Phys.* **1952**, *20*, 905−907.
(80) *The Aldrich Library of FT.-IR Spectra*; Pouchert, C. J., Ed.; Aldrich Chemical Co.: Milwaukee, WI, 1985.
(81) Bertoluzza, A.; Fagnano, C.; Morelli, A.; Gottardi, V.; Guglielmi, M. *J. Non-Cryst. Solids* **1982**, *48*, 117−128.
(82) Duchesne, J. *J. Chem. Phys.* **1948**, *16*, 1009−1010.
(83) Krishnan, K.; Stout, P. J.; Watanabe, M. In *Practical Fourier Transorm Infrared Spectroscopy—Industiral and Laboratory Analysis*; Ferraro, J. R., Krishnan, K., Eds.; Academic Press: New York, 1990.
(84) Decottignies, M.; Phalippou, J.; Zarzycki, J. *J. Mater. Sci.* **1978**, *13*, 2605−2618.
(85) Colombo, L.; Borghesi, A.; Rojas, S.; Wu, W. S. *Helv. Phys. Acta* **1989**, *62*, 742−743.
(86) Feld, R.; Cowe, P. L. *The Organic Chemistry of Titanium*; Butterworth: London, 1965.
(87) Berreman, D. W. *Phys. Rev.* **1963**, *130*, 2193-2198.
(88) Lucovsky, G.; Fitch, J. T.; Tsu, D. V.; Kim, S. S. *J. Vac. Sci. Technol. A* **1989**, *7*, 1136−1144.
(89) Almeida, R. M. *Phys. Rev. B* **1992**, *45*, 161−170.
(90) Boyd, I. W.; Wilson, J. I. B. *J. Appl. Phys.* **1982**, *53*, 4166−4172.
(91) Boyd, I. W.; Wilson, J. I. B. *Appl. Phys. Lett.* **1987**, *50*, 320−322.
(92) Boyd, I. W. *Appl. Phys. Lett.* **1987**, *51*, 418−420.
(93) Kirk, C. T. *Phys. Rev. B* **1988**, *38*, 1255−1273.
(94) Yen, Y.-S.; Wong, J. S. *Proc. SPIE-Int. Soc. Opt. Eng.* **1989**, *1145*, 205−208.
(95) Suda, Y.; Morimoto, T.; Nagao, M. *Langmuir* **1987**, *3*, 99−104.
(96) Jackson, P.; Parfitt, G. D. *Faraday Trans.* **1972**, *68*, 1443−1450.
(97) Kittel, C. *Introduction to Solid State Physics*, 6th ed.; Wiley: New York, 1986.
(98) Hamrin, K.; Johansson, G.; Gelius, U.; Nordling, C. *J. Phys. Chem. Solids* **1970**, *31*, 2669−2672.
(99) McGuire, G. E.; Schweitzer, G. K.; Carlson, T. A. *Inorg. Chem.* **1973**, *12*, 2450−2453.
(100) Tiller, H.-J.; Gobel, R.; Magnus, B.; Garschke, A.; Musil, R. *Thin Solid Films* **1989**, *169*, 159−168.
(101) Hoffman, W. P.; Ehrburger, P. *J. Anal. Appl. Pyrolysis* **1989**, *15*, 275−288.
(102) Cale, T. S.; Mahadev, V. Feature Scale Transport and Reaction During Low-Pressure Deposition Processes. In *Thin Films*; Rossnagel, S. M., Ed.; Academic Press: New York, 1996; Vol. 22; pp 175−276.
(103) Bartram, M. E.; Moffat, H. K. *J. Vac. Sci. Technol. A* **1996**, *14*, 872−878.
(104) Bartram, M. E.; Moffat, H. K. *TEOS Surface Chemistry on $SiO_2$ at CVD Temperatures and Pressures*; Proceedings of the Thirteenth International Conference on Chemical Vapor Deposition, 1996; Los Angeles Electrochemical Society Proceedings 96-5; Electrochemical Society: Pennington, NJ, 1996; pp 842−847.
(105) Lide, D. R. *Handbook of Chemistry and Physics*; CRC Press: Cleveland, OH, 1996−7; Vol. 77.
(106) Hardcastle, F. D.; Wachs, I. E. *J. Raman Spectrosc.* **1990**, *21*, 683−691.
(107) Jurgens-Kowal, T. A. Preparation and Characterization of Synthetic Mineral Surfaces: Adsorption and Thermal Decompositin of Tetraethoxysilane on Magnesium Oxide, Molybdenum, and Titanium Dioxide Surfaces. Dissertation, University of Washington, 1996.